ULTRABRIGHT NARROWBAND BUNCHED LIGHT

by

YEO XI JIE
(B.Sc. (Hons.), National University of Singapore)

A THESIS SUBMITTED FOR THE DEGREE OF

DOCTOR OF PHILOSOPHY

in

CENTRE FOR QUANTUM TECHNOLOGIES

NATIONAL UNIVERSITY OF SINGAPORE

2024

Advisor:
Professor Christian KURTSIEFER

Examiners:
Assistant Professor ZHU Di
Professor Peter HO

Declaration

I hereby declare that this thesis is my original work and it has been written by me in its entirety. I have duly acknowledged all the sources of information which have been used in the thesis.

This thesis has also not been submitted for any degree in any university previously.

Yeo Xi Jie

16 August 2024

To the children:

"The one you are waiting for to change the world... is you."

- Rachel Anne Accurso (Ms. Rachel)

Acknowledgments

The saying goes: "It takes a village to raise a child." Similarly, if we imagine the village as a bit larger, and myself as a child to this universe, then the completion of this thesis is a contribution from everyone that I interacted with in one way or another. There is something to be learned from every experience, no matter how we feel about it at the time. My parents call this "The University of Life".

First, I want to thank my teachers. Many of you I may not have seen for years, some retired, some I still bump into at NUS, but you all have laid the foundations for this thesis. I am especially grateful to the really passionate ones, how they inspired curiosity about our universe, and patiently entertained our questions beyond the syllabus. Special thanks go to the one that has taught me the longest, Christian, for taking a leap of faith and taking me under your wing when I was still this rookie Year 2 undergraduate looking for a UROPS project. I have learnt a lot from you, both in terms of soft and hard skills, and I'm grateful for the guidance you have generously offered. Who knew this journey would last 7 years? It has been an unforgettable one. I would also like to thank Duane and Valerio for enthusiastically agreeing to be part of my Thesis Advisory Committee, and making the Qualifying Exams really enjoyable with exciting discussions.

Next, I would like to thank the Technical Support and Administrative staff at CQT and Physics Department, as well as everyone else that keeps the operation going, including the staff working to keep the lights working and the place clean. Since 2017, each of you helped me in different ways, whether by teaching me how to operate workshop machinery, or helping me through some obscure administrative process which no guidelines have been established. I would also like to thank Kim Yong and Sharon for your "lobangs" whenever I needed help with equipment or expertise closer to your domain.

I am also deeply grateful to the Quantum Optics group, past and present, and even members from long ago whom I meet at conferences. Special thanks go to Matthias, Wilson, Chang Hoong, Mathias, Ale, Flo, Yifan, Darren, Justin, Peng Kian, Lijiong and Jaesuk, everyone I worked extensively with throughout my time in the Quantum Optics group, imparting their experience and knowledge to me, or learning about new things together. I also want to thank Boon Long, Chi Huan,

Janet, Adrian, Jianwei, Brenda, Ting You, Neville, Wen Xin, Vindhiya, Zifang, Ilja, Ilija, Philip, Hou Shun, Joel, Thormund and Victor for the many many interactions within and outside work. Thanks, too, to the juniors I had the chance to mentor; trying to guide you have made me taught me a great deal as well. Of course, I would like to thank all the scientific giants and forebears whose shoulders I stand.

Closer to heart, I would like to thank my still-very-active circle of friends who have stuck with me through thick and thin over a decade (or nearly so), and their family: Jared, Kailin, Bralee, Fang, Canx, Ann, Pangs, YP, Brent, Isaac, Chloe, Robby, Eugene. Also, thanks to friends/family who I had the luxury to meet through my wife: Dui, Grace, Kerr, Nigel, Sherry, JJ, Jamie and Colin. Also, thanks to, still-active friends which undertook a similar trial by fire: Derrick, Chee Chau, Sam, BiaoJin, Shiuan Jun, Zhanfeng, Mitchell, Si Min, May Inn, Zong Long, Xing Bo, Leo, Hakeem, Amin, Leo, Dian, Cass Foo and many other talented peers I got the chance to meet. I would also like to thank Ric, Charlotte, Noel, Dillon, Khim, Jun Xiang, Gen, Ivan, Jun Hao, Yaner, Shengdi, Leng Leng, Mui Huang, Shawn Peh, Jag, my F.A.S.T. Teammates, and the list of friends goes on...

Last but not least, to those closest to my heart, I really would not have pulled this off without you: Mum and Dad, Pa and Ma, Emily, Kieren, Le, Mary, Ah Tong, Ah Poh, Wahti, Auntie Poh Chu, Uncle Richard, my extended family, and of course my dearest wife Danielle and firstborn L. Thank you so much for being the light of my life. I am eternally grateful for all the thoughtfulness, patience, guidance, care and love, helping me to take care of the other things so I can focus on work. For all the times that you said you were proud of me, I felt even prouder to be your kin. Words will never fully convey my gratitude and love for you but it is because of you that I am thankful to be in this world.

There are many others I would like to thank but I will close here with one final thought. In life, things become tough, and it feels like an smothering struggle. Sometimes you feel discontent and you get blinded by wanting much more. Remember to have an open and full heart, and give your loving kindness generously while accepting the love from others gratefully. After all, in the end, quoting The Beatles:

"Love is all you need."

Contents

Abstract

Ultrabright narrowband bunched light

by

Yeo Xi Jie

Doctor of Philosophy in

National University of Singapore

Bunched light finds applications in areas such as imaging, clock synchronisation and optical ranging. These applications leverage on the temporal bunching of photons to extract timing information, similar to more "quantum" light sources, such as light from spontaneous parametric down conversion or from spontaneous emission.

This thesis describes experimental techniques to develop and characterise an ultrabright source of narrowband bunched light. The characterisation techniques, which are an extension to the work by Lebreton et al. [1, 2], are based on photon correlations between light from two output ports of an asymmetric Mach-Zehnder interferometer. Our techniques can be used to extract parameters such as the fraction of coherent light emitted by a source [3], the coherence time of a light field, and also to determine if photon bunching originates from phase fluctuations. These techniques are applied to various light sources such as lasers operating at different currents, emission from a mercury discharge lamp, laser light scattered off a rotating ground glass plate and new ultrabright bunched light source developed in this thesis.

Our ultrabright narrowband bunched light source is realised by superposing light from a continuous wave laser with itself beyond its coherence time, using an asymmetric Mach-Zehnder interferometer. Light from this source has a coherence time of $\sim 190\,\mathrm{ns}$. The mechanism of photon bunching can be attributed to phase fluctuations in the input laser, which are typically ascribed to quantum noise. From second-order photon correlations $g^{(2)}(\tau)$, the photon bunching amplitude is measured to be $g^{(2)}(0) = 1.437 \pm 0.002$. At an output power of $1\,\mathrm{mW}$, the bunched light has a spectral density of 10^{22} photons per second per nanometer linewidth, about 10^4 times higher than the best existing similar sources known to us [4]. This allows

for attenuation as much as 140 dB by the propagation media before the signal is comparable to noise in the single photon detectors. The brightness can be easily increased with a higher power laser input, and is only limited by the damage threshold of the optics.

List of Publications and Conferences

Publications relevant to this thesis that I contributed to during my PhD :

1. **Xi Jie Yeo**, Eva Ernst, Alvin Leow, Jaesuk Hwang, Lijiong Shen, Christian Kurtsiefer, Peng Kian Tan, "Direct measurement of coherent light proportion from a practical laser source.", Phys. Rev. A **109**, 013706, (2024).

2. Peng Kian Tan, **Xi Jie Yeo**, Alvin Zhen Wei Leow, Lijiong Shen, Christian Kurtsiefer, "Practical range sensing with thermal light", Phys. Rev. Applied **20**, 014060 (2023)

I have presented parts of this thesis at the following conferences:

1. [**Poster**] Direct measurement of pseudothermal light violating Siegert relation, *SPIE: Astronomical Telescopes + Insturmentation, Yokohama, Japan (2024)*
   (Publication of proceedings pending)

2. [**Poster**] Direct measurement of coherent light proportion from a laser source without spectral filtering, *CLEO: Laser Science to Photonics Applications 2024, Charlotte, North Carolina, USA. (2024)*
   (also as a Finalist for the APS DLS poster competition)

3. [**Talk**] Direct measurement of coherent light proportion from a laser source without spectral filtering, *DPG Spring Meeting, Freiburg, Germany. (2024)*

4. [**Poster**] Direct measurement of pseudothermal light violating Siegert relation, *DPG Spring Meeting, Freiburg, (2024)*

5. [**Talk**] Light source characterisation using interferometric photon correlations, *IPS Meeting 2023, Singapore. (2023)*

6. [**Poster**] Characterising the Onset of Lasing Using Interferometric Photon Correlations, *IPS Meeting 2022, Singapore. (2022)*

7. [**Poster**] Characterising the Onset of Lasing Using Interferometric Photon Correlations, *ECOC 2022, Basel, Switzerland. (2022)*

List of Figures

Chapter 1

Introduction

Photon bunching is a remarkable phenomenon where one observes a higher probability of registering photodetection events close together in time than far apart [5]. This non-uniform probability distribution can be observed from second-order photon correlations, extracted from correlating the mean photon number $N(t)$ detected from a light source at some time interval $[t, t+\delta)$, with the mean photon number $N(t+\tau)$ at another time interval $[t+\tau, t+\tau+\delta)$, with these two intervals separated by a time difference τ. Formally, this is defined as

$$g^{(2)}(\tau) = \frac{\langle N(t)N(t+\tau)\rangle}{\langle N(t)\rangle \langle N(t+\tau)\rangle}, \tag{1.1}$$

where $\langle \dots \rangle$ indicates an ensemble averaging over all t. Here, photon bunching shows up as $g^{(2)}(0) > 1$, and decays to 1 as the magnitude of the timing difference $\|\tau\|$ increases.

Light exhibiting photon bunching can also be referred to as bunched light [6]. Examples of bunched light sources include stars [7–9], discharge lamps [10–13], scattering of light off particles [14–17] and rotating ground glass [18–25], superluminescent diodes [26], pulsed lasers [27], laser amplifiers [28], lasers operating at subthreshold [4], spontaneous parametric down conversion in nonlinear crystals [29–33] and atomic vapours [34].

Recently, bunched light finds applications in sensing, such as imaging [35–37], ranging [4, 38, 39], and clock synchronisation [40, 41]. These applications leverage on the photon bunching property from which timing information can be extracted, such as the time-of-flight of the photons.

Among the bunched light sources applied to sensing, there is a growing interest in sources where photon bunching specifically originates from quantum processes [4,

37, 39–41]. Examples of these quantum processes include spontaneous emission [42], where a photon is produced by the radiative decay of an emitter, and spontaneous parametric down conversion [43, 44], where a single photon is converted to multiple photons via a nonlinear optical medium. Due to the indeterminacy of quantum mechanics, these processes occur in a manner considered to be "truly" random [45]. This contrasts with pseudo-randomness where the apparently random sequence generated this way can be accurately predicted if the mechanism or algorithm to generate the sequence is identically replicated.

Applied to sensing, the "true" random occurrences of photon bunching from quantum processes can be leveraged upon as a natural means to suppress cross-talk, even between identically constructed sources. Specifically, a photon bunching signature would be observed when correlating detection events of photons originating from the same light source, and would not be observed when correlating detection events of photons originating from different light sources. This enables a clearer distinction between signals when using identically constructed sources in proximity.

Despite the benefits of cross-talk suppression, sensing techniques using such bunched light sources are limited by a minimum measurement time. This can be interpreted as the time needed to register enough photodetection events for clear observation of photon bunching at some level of statistical confidence. Especially crucial in time-sensitive applications such as the detection of transient events and the observation of dynamic processes, the minimum measurement time has to be significantly shorter than the timescales of these events and processes. To achieve a short measurement time, two properties of the bunched light source need to be optimised: high output brightness and a large photon bunching amplitude.

A high output brightness of the bunched light source is necessary in sensing applications to withstand channel losses in the propagation media, and if applicable, scattering losses from a target of interest. This ensures sufficient illumination of the detectors by the bunched light source for an appreciable photodetection rate after losses.

On the other hand, the photon bunching amplitude contrasts the detection of photoevents originating from bunched light close together in time against "accidental" photoevents close together in time. However, in general, there are no straightforward ways of increasing the photon bunching amplitude, although there are recent works

suggesting methods via amplitude modulation of light [46–48]. Even so, amplitude modulation techniques would not apply to bunched light sources with photon bunching from quantum effects, as it involves an additional source of modulation, defeating the purpose of using the bunched light for its intrinsic randomness.

The bandwidth of the bunched light also affects the minimum measurement time required to resolve the photon bunching. Typically, the bandwidth of a bunched light source is inversely proportional to the characteristic timescale of photon bunching [5, 6]. In other words, a broadband bunched light source has a short characteristic timescale of photon bunching. When this timescale is short compared to the temporal resolution of the photodetectors, the convolution of the photon bunching signature with the temporal response of the detectors results in a reduction in photon bunching amplitude observed [49]. Consequently, the reduced photon bunching amplitude requires more photodetection events before it can be confidently resolved. Following this reasoning, a sufficiently narrowband bunched light is needed for a correspondingly long characteristic timescale of photon bunching which circumvents the reduction in photon bunching amplitude due to convolution with temporal response of the detectors.

Thus, the bandwidth and output brightness are the actual limitations to the sensing application. These two parameters can be jointly characterised by the spectral density of the light source, with a high spectral density being desirable here. The discussion thus far motivates for techniques to construct bunched light sources with high spectral density and photon bunching originating from quantum effects for more demanding sensing applications.

Thesis outline

In this thesis, we describe experimental techniques to develop and characterise an ultrabright source of narrowband bunched light. Our bunched light source is realised by superposing light from a continuous wave laser with itself beyond its coherence time, using an asymmetric Mach-Zehnder interferometer. This utilises the intrinsic phase fluctuation in the laser, commonly attributed to quantum noise from the uncertainty in the energy of the light and its emitter [50], to achieve the photon bunching. Following this argument, we ascribe the photon bunching to quantum

noise. On the other hand, the brightness and the narrow bandwidth of the input laser makes the photon bunching easily resolvable even with slow detectors. Prior to its demonstration as a bunched light source, this technique was used as a method to generate random intensity spikes as part of a quantum random number generator [51, 52].

To characterise the bunched light source, we develop techniques to extract parameters such as the fraction of coherent light emitted by a laser, the coherence time of the light, and also to determine if photon bunching originates from phase fluctuations. These characterisation techniques, which are extensions of the work by Lebreton et al. [1, 2], are based on the correlation of photoevents detected at the output ports of an asymmetric Mach-Zehnder interferometer. We present an overview of these correlations, referred to as interferometric photon correlations $g^{(2X)}(\tau)$, in Chapter 2.

We extended the use of interferometric photon correlations $g^{(2X)}(\tau)$ in Chapter 3 to develop a technique to measure the fraction of coherent light emitted by a laser source which determines the maximum photon bunching amplitude achievable by the ultrabright bunched light source. Using interferometric photon correlations $g^{(2X)}(\tau)$, we are also able to measure the coherence time of the coherent light emitted by the laser.

In Chapter 4, we use interferometric photon correlations $g^{(2X)}(\tau)$ to determine if photon bunching is related to the phase fluctuations in a bunched light source. To do this, we directly observe the difference between the second-order photon correlation $g^{(2)}(\tau)$ and the interferometric visibility $\|g^{(1)}(\tau)\|$ of a light source which appears around $\tau = 0$ in its interferometric photon correlation $g^{(2X)}(\tau)$. Using this technique, we report our findings that the photon bunching observed from laser light scattered off a rotating ground glass plate is not purely from its phase fluctuations. In contrast, from the interferometric photon correlation $g^{(2X)}(\tau)$ of the green emission from a mercury discharge lamp around 546 nm, its photon bunching effect appears to be related to its phase fluctuations. Therefore, the emission from the mercury discharge lamp is indeed a source of thermal light, as demonstrated in many past experiments.

In Chapter 5, we present our bunched light source, where we reach a bunching amplitude of $g^{(2)}(0) = 1.437 \pm 0.002$, which is close to the predicted value of $g^{(2)}(0) = 1.44$ from the fraction of coherent light emitted by the input laser. At

an output power of 1 mW, this light source has a spectral density of about 10^{22} photons/sec/nm, making it 10^4 times brighter than the brightest bunched light known to us, which is based on a laser operating below its lasing threshold [4]. From its interferometric photon correlation $g^{(2X)}(\tau)$, the photon bunching effect appears to be related to the phase fluctuations of the laser, which can be attributed to quantum noise [50]. We conclude the thesis with the summaries and outlook from these experiments in Chapter 6.

Chapter 2

Interferometric photon correlations

To characterise the bunched light source, we require techniques to characterise its coherence time, and fraction of coherent light emitted, as well as a method to determine if the photon bunching is related to the phase fluctuations. To measure coherence time, a common technique is to use a scanning Michelson or Mach-Zehnder interferometer. For the lasers we use in our experiments, they have a bandwidth on the order of MHz, corresponding to a coherence time on the order of 100 ns. Using a scanning interferometer to extract the coherence time of these lasers would require scanning a path length on the order of 100 m, which may be challenging on the length scale of a laboratory.

On the other hand, to measure the fraction of coherent light, second-order photon correlations, which measures the timing separation of photons from a source, may be used [53–57] This would require spectral filtering if there is a mixture of coherent with broadband thermal light [58], which would fail to characterise the full emission of a laser [3]. Hence, we require alternative techniques for these characterisations.

To characterise our light sources, we use and develop techniques that are based on interferometric photon correlations $g^{(2X)}(\tau)$. Interferometric photon correlations $g^{(2X)}(\tau)$ developed by the group of Lebreton et al. [1], are timing correlations extracted from photoevents detected at the output ports of an asymmetric Mach-Zehnder interferometer, and contains both features of second-order photon correlations $g^{(2)}(\tau)$ and interferometric visbility $\left\|g^{(1)}(\tau)\right\|$. It was previously used to distinguish an incoherent light source from a coherent light source undergoing amplitude modulation [2]. Similar techniques featuring the sending of light through an asymmetric Mach-Zehnder interferometer were used to study organic molecules

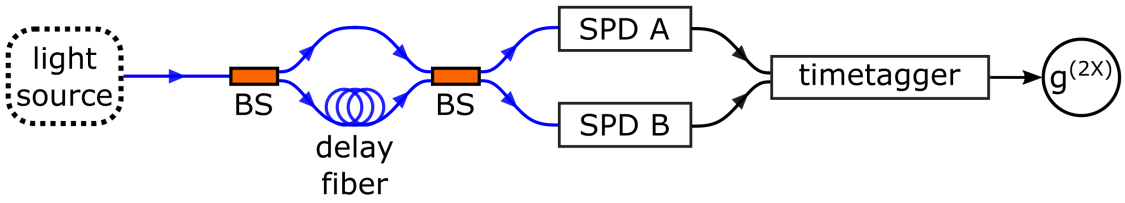

Figure 2.1: Setup to determine the interferometric photon correlation $g^{(2X)}(\tau)$. Light from the source under test is sent through an asymmetric Mach-Zehnder interferometer, formed by two optical path from two output ports, indexed as A and B. At each output port, photoevents are detected using single-photon detectors (SPD), where photodetection events are timetagged. A correlation between detection timings would extract interferometric photon correlations $g^{(2X)}$. For high enough power, conventional PIN photodiodes may replace the single-photon detectors, and its time-varying power recorded by an analog to digital converter.
BS: Beam splitter

in a solid matrix undergoing spectral diffusion [59], and to characterise the phase noise of a laser [60]. In this Chapter, we provide an introduction to interferometric photon correlations.

A schematic setup to extract interferometric photon correlations is shown in Figure 2.1. The light source under test has an electric field $E(t)$ that is sent through an asymmetric Mach-Zehnder interferometer. When light enters the interferometer, a beamsplitter divides the beam into two propagation modes of equal intensity. Each mode then propagates through individual paths of different length before spatially overlapping again at a second beam splitter. The path difference creates a propagation delay Δ between the two light fields before recombining on a second splitter and is significantly longer than the coherence time τ_c of the light source. With the long propagation delay, the interfering fields $E(t)$ and $E(t+\Delta)$ are uncorrelated in time when they spatially overlap at a second beamsplitter, i.e.

$$\langle E^*(t)E(t+\Delta)\rangle = 0, \tag{2.1}$$

where $\langle \dots \rangle$ denotes the expectation value of the terms enclosed over the variable t.

The resultant light fields at the output ports A, B of the interferometer are

$$E_{A,B}(t) = \frac{E(t) \pm E(t+\Delta)}{\sqrt{2}}, \tag{2.2}$$

with a sign difference due to the π phase difference acquired by one of the fields at the beamsplitter where the two fields recombine [61].

In general, the intensity of the light field at each output $I_{A,B}(t) = E^*_{A,B}(t)E_{A,B}(t)$ are measured and correlated. To extract interferometric photon correlations

$$g^{(2X)}(\tau) = \frac{\langle E^*_A(t)E^*_B(t+\tau)E_B(t+\tau)E_A(t)\rangle}{\langle E^*_A(t)E_A(t)\rangle\langle E^*_B(t)E_B(t)\rangle}\,. \tag{2.3}$$

If single-photon detectors are used to measure the intensity at each output port A, B of the interferometer, photoevents are detected over an integration time T with the detection timings logged by the time tagger. The number of "single" photoevents detected at each detector at output port A, B over the measurement time T, is denoted by $S_{A,B}$ respectively. To extract interferometric photon correlations $g^{(2X)}(\tau)$, we compute the timing difference between photodetection timings pairwise, and count the number of pairs, referred to as coincidences $C(\tau)$, that are within a timing difference interval of $[\tau, \tau+\delta)$, where δ is the size of each timing interval. We assume the coincidences $C(\tau)$ in each time interval follows a Poissonian distribution, so we assign an error $\sqrt{C(\tau)}$ to the measured coincidences $C(\tau)$ in each time interval.

The mean coincidence rate within each timing difference interval, $C(\tau)\delta/T$, is then normalised by the product of the mean photoevents rate at each detector

$$\begin{aligned} g^{(2X)}(\tau) =& \frac{C(\tau)\delta/T}{(S_A\delta/T)\,(S_B\delta/T)} \\ =& \frac{C(\tau)\,T}{S_A\,S_B\,\delta}. \end{aligned} \tag{2.4}$$

This method of extracting photon correlations from timestamps can also be used to extract second-order photon correlations $g^{(2)}(\tau)$, but with a different optical setup, shown in Figure 2.2.

Alternatively, for light emerging from the interferometer with sufficiently high optical power, the time-varying power $P_{A,B}(t)$ at each output port A, B of the interferometer can be measured with conventional PIN photodiodes, instead of single photon detectors, and recorded with an oscilloscope. The sampling discretises the time-varying power to $P_{A,B}(t_m)$ with a step size of δ, so $t_m = m\delta$. The interferometric

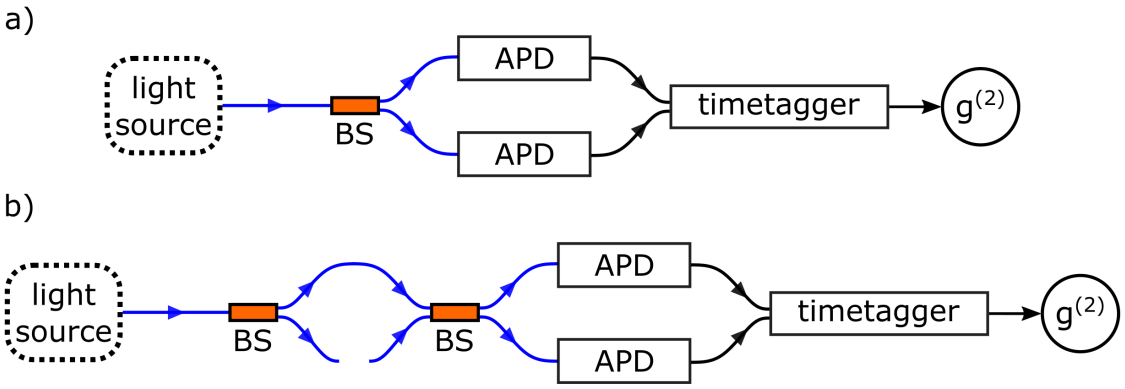

Figure 2.2: Variations of setups used to extract second-order photon correlations $g^{(2)}(\tau)$ in this Thesis. (a) conventional Hanbury-Brown Twiss type configuration (b) Hanbury-Brown Twiss type interferometer by disconnection or obstruction to one arm of an asymmetric Mach-Zehder inteferometer in a setup to extract interferometric photon correlation $g^{(2X)}(\tau)$. In both cases, light from the source under test is sent to a beam splitter (BS) which splits the light field into two output ports. At each output port, photoevents are detected using avalanche photodiodes (APD), where detection timings are logged by a timestamp unit. A correlation between detection timings similar to the method described to extract interferometric photon correlations $g^{(2X)}(\tau)$ in Equation 2.4.

photon correlation can then be evaluated from $P_{A,B}(t_m)$:

$$\begin{aligned} g^{(2X)}(\tau) =& \frac{\sum^l P_A(t_l) P_B(t_l+\tau)\,\delta/T}{(\sum^m P_A(t_m)\delta/T)\;(\sum^n P_B(t_n+\tau)\delta/T)} \\ =& \frac{\sum^l P_A(t_i) P_B(t_l+\tau)}{\sum^m P_A(t_m)\sum^n P_B(t_n+\tau)}\frac{T}{\delta} \end{aligned} \tag{2.5}$$

For readability and consistency, we analyse the interferometric photon correlations $g^{(2X)}(\tau)$ in terms of electric fields for the remainder of this thesis. The results are the same when using quantum mechanical operators of the light field [62].

Using Equation 2.2, $g^{(2X)}(\tau)$ can be expanded into several terms:

$$\begin{aligned} g^{(2X)}(\tau) = \frac{1}{4}[&\langle E^*(t)E^*(t+\tau)E(t+\tau)E(t)\rangle \\ &+ \langle E^*(t+\Delta)E^*(t+\tau+\Delta)E(t+\tau+\Delta)E(t+\Delta)\rangle \\ &+ \langle E^*(t+\Delta)E^*(t+\tau)E(t+\tau)E(t+\Delta)\rangle \\ &+ \langle E^*(t)E^*(t+\tau+\Delta)E(t+\tau+\Delta)E(t)\rangle \\ &- \langle E^*(t+\Delta)E^*(t+\tau)E(t+\tau+\Delta)E(t)\rangle \\ &- \langle E^*(t)E^*(t+\tau+\Delta)E(t+\tau)E(t+\Delta)\rangle]\,, \end{aligned} \tag{2.6}$$

where we omitted terms in the expansion with an unequal number of fields and conjugates containing Δ, as these terms average out to zero when computing their expectation values. For easy normalisation, we have also assumed that $\langle E_A^*(t)E_A(t)\rangle = \langle E_B^*(t)E_B(t)\rangle = \langle E^*(t)E(t)\rangle = 1$ in the denominator of Equation 2.6.

The terms in Equation 2.6 can be simply written in terms of the interferometric visibility

$$\left\|g^{(1)}(\tau)\right\| = \left\|\frac{\langle E^*(t)E(t+\tau)\rangle}{\langle E^*(t)E(t)\rangle}\right\| \tag{2.7}$$

and second-order photon correlations

$$g^{(2)}(\tau) = \frac{\langle E^*(t)E^*(t+\tau)E(t+\tau)E(t)\rangle}{\langle E^*(t)E(t)\rangle\langle E^*(t)E(t)\rangle}\,. \tag{2.8}$$

The first two terms in Equation 2.6 equal to second-order photon correlations $g^{(2)}(\tau)$, the middle two terms equal to second-order photon correlations $g^{(2)}$, time-shifted by $-\Delta$ and $+\Delta$, respectively, and the last-two terms equal to interferometric visibility-square $\left\|g^{(1)}(\tau)\right\|^2$. Therefore, we rewrite Equation 2.6

$$\begin{aligned} g^{(2X)}(\tau) =& \frac{1}{4}\left[g^{(2)}(\tau+\Delta) + g^{(2)}(\tau-\Delta)\right] \\ &+ \frac{1}{2}\left[g^{(2)}(\tau) - \left\|g^{(1)}(\tau)\right\|^2\right]. \end{aligned} \tag{2.9}$$

2.1 Coherent and thermal light

To illustrate the characteristic features in interferometric photon correlations $g^{(2X)}(\tau)$, we show theoretical traces in Figure 2.3 for coherent and thermal light

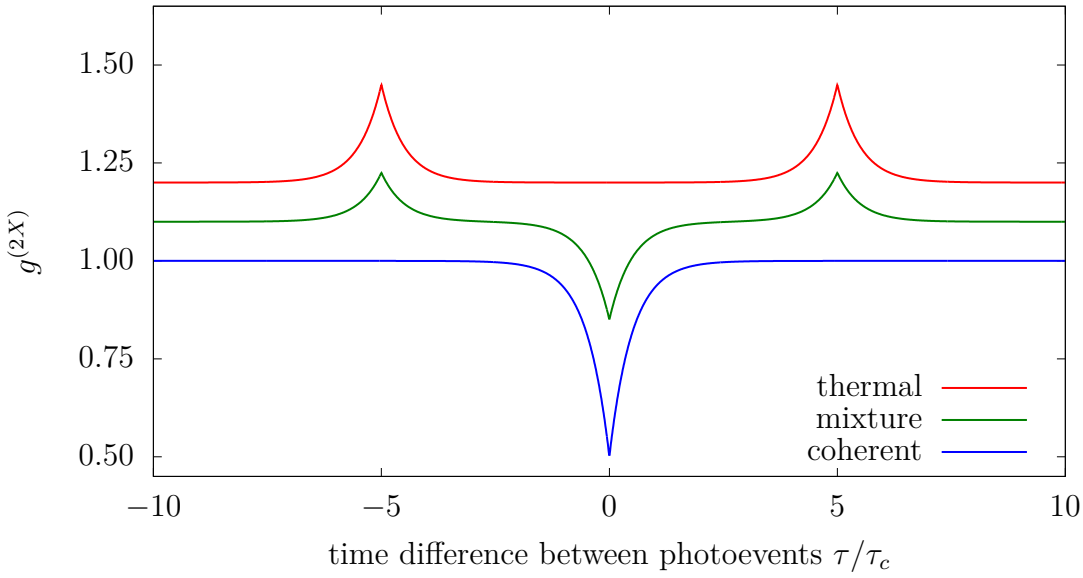

Figure 2.3: Theoretical interferometric photon correlations $g^{(2X)}(\tau)$ for thermal light (top, red), a mixture of thermal and coherent light (middle, green) and coherent light (bottom, blue). The horizontal axis is represented in terms of multiples of the characteristic timescale of the light τ_c. We have used a propagation delay $\Delta = 5\,\tau_c$ in these plots. The plots were vertically offset by 0.2 for the top plot and 0.1 for the middle plot for clarity.

with Lorentzian spectral lineshapes as an example. Here, we have assumed that the detectors used have a timing resolution shorter than the characteristic timescale τ_c of the light source, which allows the "bunching" and dip signatures to be resolved. However, for a limited timing resolution, these features would flatten due to a convolution with the detector's response [49].

As a light source's interferometric visibility $\|g^{(1)}(\tau)\|$ is the Fourier transform of its lineshape, light sources with a Lorentzian spectral lineshape would have a corresponding $\|g^{(1)}(\tau)\|$ with an exponential decay profile [63, 64],

$$\left\|g^{(1)}(\tau)\right\| = e^{-\left\|\frac{\tau}{\tau_c}\right\|}, \tag{2.10}$$

where τ_c is a characteristic time constant inversely related to the spectral linewidth.

For thermal light, such as light from an ensemble of emitters undergoing spontaneous emission, the Siegert relation [65] connects the second-order photon correlation $g^{(2)}(\tau)$ to the interferometeric visibility $\|g^{(1)}(\tau)\|$:

$$g^{(2)}(\tau) = 1 + \left\|g^{(1)}(\tau)\right\|^2. \tag{2.11}$$

We present a derivation of the Siegert relation in Section 4.1. Using this relationship, the second term in Equation 2.9 equals to 1, resulting in

$$g^{(2X)}(\tau) = \frac{1}{2} + \frac{1}{4}\left[g^{(2)}(\tau+\Delta) + g^{(2)}(\tau-\Delta)\right]. \tag{2.12}$$

As shown in Figure 2.3 top, the plot is constant at $g^{(2X)}(\tau \approx 0) = 1$, with two "bunching" signatures centred around the propagation delay $\tau = \pm\Delta$, where we have used $\Delta = 5\,\tau_c$. The peaks of these "bunching" signatures are $g^{(2X)}(\pm\Delta) = 1.25$, assuming an ideal thermal light $g^{(2)}(0) = 2$.

For coherent light, the second-order photon correlation is $g^{(2)}(\tau) = 1$, which results in a corresponding interferometric photon correlation

$$g^{(2X)}(\tau) = 1 - \frac{1}{2}\left\|g^{(1)}(\tau)\right\|^2. \tag{2.13}$$

Figure 2.3, bottom, shows this dip feature centered around $\tau = 0$, with its lowest point at of $g^{(2X)}(0) = 0.5$.

We expect the second-order photon correlation $g^{(2X)}(\tau)$ for a mixture of thermal and coherent light to look similar to Figure 2.3 middle. The features of interferometric photon correlation $g^{(2X)}(\tau)$ are expected to have a reduced dip amplitude $0.5 < g^{(2X)}(0) < 1$, and the "bunching" signatures at $\tau = \pm\Delta$ to have a reduced height.

2.2 Comparing $g^{(2)}(\tau)$ and $\|g^{(1)}(\tau)\|^2$

The photon bunching of a light source is characterised by second-order photon correlations $g^{(2)}(\tau)$, while the phase fluctuations of the light source can be characterised by its interferometeric visibility $\|g^{(1)}(\tau)\|$. Therefore, a comparison between second-order photon correlations $g^{(2)}(\tau)$ and the interferometeric visibility $\|g^{(1)}(\tau)\|$ sheds insights on the relationship, if any, between the phase fluctuations of the light source and its photon bunching.

The difference between a light source's interferometeric visibility $\|g^{(1)}(\tau)\|$ and second-order photon correlation $g^{(2)}(\tau)$, shows up as a feature around $\tau \approx 0$ in interferometric photon correlations $g^{(2X)}(\tau)$, allowing a direct comparison between the two. Therefore, by observing the features around $\tau \approx 0$ in interferometric photon correlations $g^{(2X)}(\tau)$, we make comparisons of the temporal profile and timescales between phase fluctuations and photon bunching.

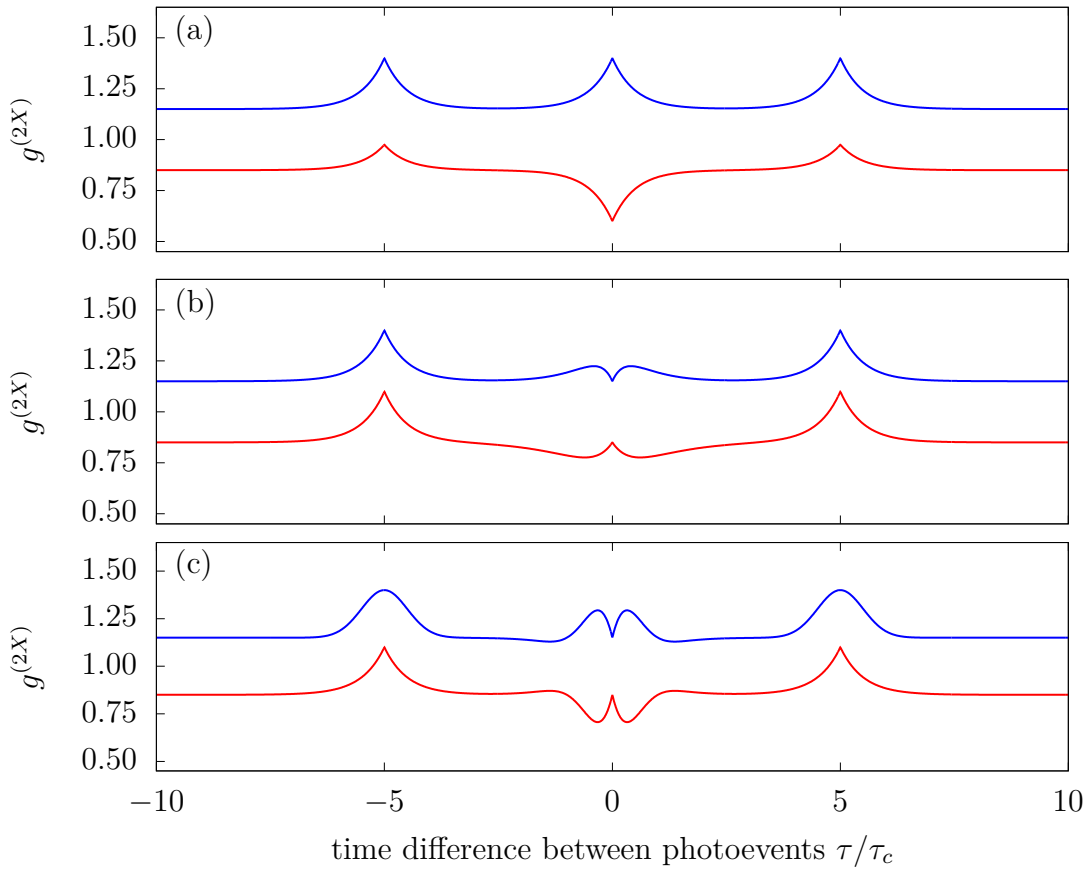

Figure 2.4: Theoretical interferometric photon correlations $g^{(2X)}(\tau)$ with different (a) amplitudes, (b) timescales and (c) temporal profiles between second-order photon correlation $g^{(2)}(\tau)$ and interferometeric visibility-square $\|g^{(1)}(\tau)\|^2$. (a) Amplitude $g^{(2)}(0)-1$ that is 2 times (top,blue) $\|g^{(1)}(0)\|^2$ and Amplitude $g^{(2)}(0)-1$ that is 0.5 times $\|g^{(1)}(0)\|^2$ (red,bottom). (b) Characteristic timescale of $g^{(2)}(\tau)$ that is 0.5 times longer (top,blue)/ shorter (red,bottom) compared to the timescale of $\|g^{(1)}(\tau)\|^2$. (c) Same timescale and amplitude, but $g^{(2)}(\tau)$ is a Gaussian profile and $\|g^{(1)}(\tau)\|^2$ is a two-sided exponential decay (top,blue), and vice-versa (red,bottom). For clarity, the top, blue and bottom, red plots have been offset vertically by ± 0.15 respectively. We have used a propagation delay $\Delta = 5\,\tau_c$ in these plots.

For second-order photon correlation $g^{(2)}(\tau)$ and interferometeric visibility $\|g^{(1)}(\tau)\|$ with the same temporal profile and timescale but different amplitudes, the difference between the two is linear sum of two distributions with the same temporal profile and timescale, which can be factored out, equating to a constant term plus a scalar multiple of the temporal profile. Correspondingly, this shows up as a unimodal distribution the interferometric photon correlations $g^{(2X)}(\tau)$ around $\tau \approx 0$, as shown in Figure 2.4(a). Furthermore, when the amplitudes of interferometeric visibility $\|g^{(1)}(\tau)\|$ and second-order photon correlation $g^{(2)}(\tau)$ are the same, these two function cancels out exactly, leaving behind a constant. Therefore, the corresponding interferometric photon correlations $g^{(2X)}(\tau)$ around $\tau \approx 0$ would be a constant function, with an example being thermal light in Fig 2.4 top.

However, when the second-order photon correlation $g^{(2)}(\tau)$ and interferometeric visibility-square $\|g^{(1)}(\tau)\|^2$ do not have the same temporal profile or timescale, there would be a residual difference $g^{(2)}(\tau) - \|g^{(1)}(\tau)\|^2$. This shows up in the interferometric photon correlations $g^{(2X)}(\tau)$ as a bimodal distribution centered around $\tau = 0$. We show in Figure 2.4(b), the interferometric photon correlations $g^{(2X)}(\tau)$ in scenarios where the second-order photon correlation $g^{(2)}(\tau)$ and interferometeric visibility-square $\|g^{(1)}(\tau)\|^2$ have different timescales, and in Figure 2.4(c), when they have different temporal profiles.

Summary

We have established the theoretical fundamentals of measuring interferometric photon correlations $g^{(2X)}(\tau)$, where photon or intensity correlations between the two output ports of an asymmetric Mach-Zehnder interferometer were extracted. We showed some theoretical examples of interferometric photon correlations $g^{(2X)}(\tau)$ for coherent and thermal light, and predicted the interferometric photon correlation $g^{(2X)}(\tau)$ for an arbitrary mixture of coherent and thermal light. However, a relationship between interferometric photon correlation $g^{(2X)}(\tau)$ and the proportion of coherent light in a mixture has not been previously established. In Chapter 3, we present our method of measuring this proportion using interferometric photon correlations $g^{(2X)}(\tau)$, and also use it to extract the characteristic timescale of the coherent light's interferometric visibility $\|g^{(1)}(\tau)\|$ to extract its frequency bandwidth.

We also showed how interferometric photon correlations $g^{(2X)}(\tau)$ compare the second-order photon correlation $g^{(2)}(\tau)$ and interferometric visibility-square $\|g^{(1)}(\tau)\|^2$. A unimodal distribution in interferometric photon correlations $g^{(2X)}(\tau)$ around $\tau \approx 0$ indicates a similar temporal profile between second-order photon correlation $g^{(2)}(\tau)$ and interferometric visibility $\|g^{(1)}(\tau)\|$, whereas if they differ in temporal profile or characteristic timescales, a multimodal distribution would be seen.

The interferometric visibility $\|g^{(1)}(\tau)\|$ characterises the phase fluctuations in a light source, while second-order photon correlation $g^{(2)}(\tau)$ characterises the photon bunching phenomenon. Therefore, the difference between $\|g^{(1)}(\tau)\|$ and $g^{(2)}(\tau)$ that is directly compared in interferometric photon correlations $g^{(2X)}(\tau)$ near $\tau \approx 0$ can be used to infer if the photon bunching phenomenon is related to the phase fluctuations. We shall apply this technique to the light sources presented in Chapter 4 and 5.

Chapter 3

Characterising the emission of a laser

In the search of bright sources of bunched light, we have a closer look to lasers. In principle, lasers mostly emit coherent light that shows no photon bunching and have an extremely high spectral brightness. Thus, it is appealing to develop methods that can generate bunched light using laser light as an input, while maintaining its spectral brightness.

In reality, lasers may not emit fully coherent light, and may contain residual broadband incoherent light, or emits into multiple longitiudinal modes which are incoherent with respect to each other. Using lasers with such features to generate bunched light may influence some parameters of the bunched light such as the photon bunching's characteristic timescale or amplitude. Thus, some characterisation of the laser emission is necessary, in particular, the fraction of its emission that is contributed by coherent light, and the coherence time of the laser.

To characterise the fraction of coherent light, an approach may be via second-order photon correlations $g^{(2)}(\tau)$, which was used to observe the transition to lasing in lasers [53–57]. However, second-order photon correlations $g^{(2)}(\tau)$ does not distinguish coherent light from broadband incoherent light well, as both shows $g^{(2)}(0) \approx 1$. Spectral filters may be used to distinguish between incoherent and coherent light, but light outside the filter transmission window is discarded. This limits the full characterisation of the emission.

On the other hand, a common way of measuring coherence time is by sending the light through a scanning Michelson or Mach-Zehnder interferometer. As the bandwidth and coherence time are inversely related, lasers typically have bandwidths

on the order of MHz, with a corresponding coherence time on the order of 100 ns. If traditional techniques to measure coherence times are used, a scanning path length on the order of 100 m is needed. Scanning through such distances is unfeasible in a typical laboratory.

Towards constructing a bunched light source from a laser, methods to characterise the emission from a laser are necessary. In this Chapter, we present a technique to quantify the fraction of coherent light emitted by a laser diode [3], using interferometric photon correlations $g^{(2X)}(\tau)$. The coherence time and frequency bandwidth of the emission may also be extracted from the interferometric photon correlation $g^{(2X)}(\tau)$.

3.1 Connecting coherent light fraction to $g^{(2X)}(\tau)$

In Section 2.1, we have shown that fully coherent light and thermal light can be distinguished through the zero-time delay interferometric photon correlations $g^{(2X)}(0)$. A value of $g^{(2X)}(0) = 1$ indicates thermal light while $g^{(2X)}(0) = 0.5$ is indicates coherent light. This suggests that partially coherent light leads to $0.5 < g^{(2X)}(0) < 1$. We now try to extract the fraction of coherent light ρ in the light source.

3.1.1 Modelling a mixture containing coherent light

We consider the light emitted by the laser diode to be neither completely coherent nor thermal. We assume that light emitted by the laser is a mixture of a coherent light field E_{coh} and a light field E_{unc} uncorrelated to E_{coh}. The nature of E_{unc} can be coherent, thermal, or a coherent-thermal mixture. As E_{unc} may also be a mixture of uncorrelated coherent modes, E_{coh} here represents the coherent mode in the mixture with the highest intensity.

We model the light field mixture with an electric field

$$E_{\text{mix}}(t) = \sqrt{\rho}E_{\text{coh}}(t) + \sqrt{1-\rho}E_{\text{unc}}(t)\,, \tag{3.1}$$

where ρ is the fraction of optical power emitted from the brightest coherent mode, and the respective light field terms are normalised such that $\|E_{\text{mix}}\| = \|E_{\text{coh}}\| = \|E_{\text{unc}}\|$.

For physically possible solutions, the fraction of coherent light ρ must be real valued and $0 \leq \rho \leq 1$.

3.1.2 Relationship between $g^{(2X)}(0)$ and ρ

We extract the fraction of coherent light ρ from the light field mixture interferometric photon correlation $g^{(2X)}_{\text{mix}}(\tau)$ at $\tau = 0$. To do this, we use Equation 2.9, which requires the interferometric visibility-squared of $E_{\text{mix}}(t)$

$$\begin{aligned}\left\|g^{(1)}_{\text{mix}}(\tau)\right\|^2 = \rho^2 \left\|g^{(1)}_{\text{coh}}(\tau)\right\|^2 + (1-\rho)^2 \left\|g^{(1)}_{\text{unc}}(\tau)\right\|^2 \\ + 2\rho(1-\rho)\,\Re[g^{(1)}_{\text{coh}}(\tau)\, g^{(1)*}_{\text{unc}}(\tau)] \\ + 2\rho(1-\rho)\,\Re[g^{(1)}_{\text{coh}}(\Delta)\, g^{(1)*}_{\text{unc}}(\Delta)]\,,\end{aligned} \tag{3.2}$$

and second-order photon correlation of $E_{\text{mix}}(t)$

$$\begin{aligned}g^{(2)}_{\text{mix}}(\tau) = \rho^2\, g^{(2)}_{\text{coh}}(\tau) + (1-\rho)^2\, g^{(2)}_{\text{unc}}(\tau) \\ + 2\rho(1-\rho)\left[1 + \Re[g^{(1)}_{\text{coh}}(\tau)\, g^{(1)*}_{\text{unc}}(\tau)\right]\,.\end{aligned} \tag{3.3}$$

where the subscripts indicate the $g^{(1)}(\tau)$ or $g^{(2)}(\tau)$ of the coherent, uncorrelated or mixture of light fields in the same convention as in Equation 3.1, and $g^{(1)*}(\tau)$ is the complex conjugate of $g^{(1)}(\tau)$. We note that for a propagation delay Δ significantly longer than the coherence time of the light source, $g^{(1)}(\Delta) \approx 0$.

Using Equation 3.2 and 3.3,the interferometric photon correlation of the mixture light field at zero time difference becomes

$$\begin{aligned}g^{(2X)}_{\text{mix}}(0) =& \frac{1}{4}[g^{(2)}_{\text{mix}}(\Delta) + g^{(2)}_{\text{mix}}(-\Delta) \\ &+ 2(\rho^2\, g^{(2)}_{\text{coh}}(0) + (1-\rho)^2\, g^{(2)}_{\text{unc}}(0) + 2\rho(1-\rho)) \\ &- 2(\rho^2 \left\|g^{(1)}_{\text{coh}}(0)\right\|^2 + (1-\rho)^2 \left\|g^{(1)}_{\text{unc}}(0)\right\|^2)]\,.\end{aligned} \tag{3.4}$$

.

We further use $g^{(2)}_{\text{coh}}(0) = 1$ for coherent light, $g^{(2)}_{\text{coh}}(\Delta) \approx 1$ for a propagation Δ significantly longer than coherence time of the light source and assume $\left\|g^{(1)}_{\text{unc}}(0)\right\| \approx 1$ for an interferometer with good visibility which reduces Eqn 3.4 to

$$g^{(2X)}_{\text{mix}}(0) = 2\rho - \frac{3\rho^2}{2} + \frac{(1-\rho)^2}{2} g^{(2)}_{\text{unc}}(0), \tag{3.5}$$

with $g^{(2X)}_{\text{mix}}(0)$ being measured in our experiments and $g^{(2)}_{\text{unc}}(0)$ as a parameter.

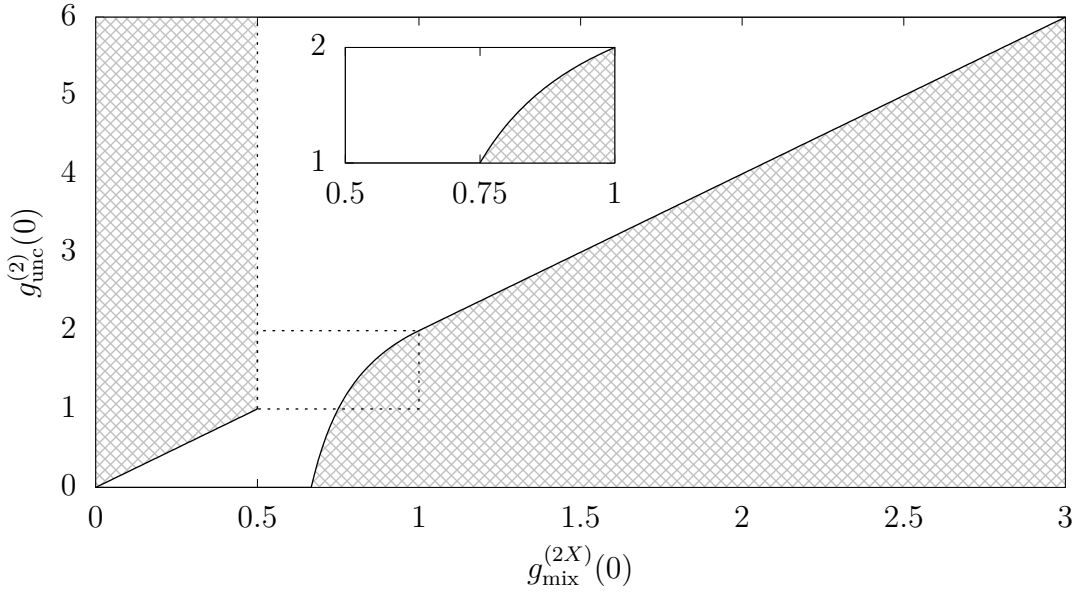

Figure 3.1: Combinations of $g^{(2X)}_{\mathrm{mix}}(0)$ and $g^{(2)}_{\mathrm{unc}}(0)$. The shaded areas demarcate the combinations that give non-physical solutions of ρ. Inset shows the possible combinations of $g^{(2X)}_{\mathrm{mix}}(0)$ and $g^{(2)}_{\mathrm{unc}}(0)$ for this experiment.

3.1.3 Relationships bounding $g^{(2)}_{\mathbf{unc}}(0)$ to $g^{(2X)}_{\mathbf{mix}}(0)$

For physically possible solutions, other than the constraints that $0 \leq \rho \leq 1$ and ρ is real-valued, we also require $g^{(2X)}_{\mathrm{mix}}(0)$, $g^{(2)}_{\mathrm{unc}}(0) \geq 0$. We also note that for $1 < g^{(2)}_{\mathrm{unc}} < 2$ and $0.5 < g^{(2X)}_{\mathrm{mix}} < 1$, one of the solutions to Equation 3.5, always results in $\rho \leq 0.5$, which does not fully reflect the possible range $0 \leq \rho \leq 1$, and hence rejected. With these constraints, this results in lower bounds

$$g^{(2)}_{\mathrm{unc}}(0) \geq \begin{cases} 0\,, & g^{(2X)}_{\mathrm{mix}}(0) \leq \frac{2}{3} \\ 3 + \frac{1}{1-2g^{(2X)}_{\mathrm{mix}}(0)}, & g^{(2X)}_{\mathrm{mix}}(0) \in [\frac{2}{3}, 1] \\ 2g^{(2X)}_{\mathrm{mix}}(0) & g^{(2X)}_{\mathrm{mix}}(0) \geq 1 \end{cases}, \tag{3.6}$$

and upper bounds for $g^{(2X)}_{\mathrm{mix}}(0) \in [0, \frac{1}{2})$

$$g^{(2)}_{\mathrm{unc}}(0) \leq 2g^{(2X)}_{\mathrm{mix}}(0), \tag{3.7}$$

which is shown in Figure 3.1.

We further assume that the uncorrelated light field is a mixture of coherent light $[g^{(2)}(\tau) = 1]$, and thermal light $[g^{(2)}(0) = 2]$ which bound its second-order photon

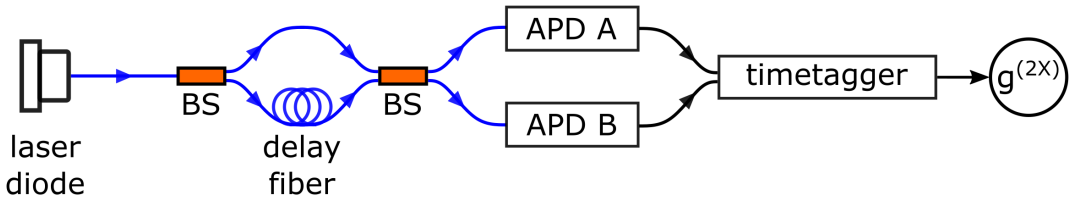

Figure 3.2: Setup to extract the fraction ρ of coherent light emitted by a laser diode. Light from the laser light is sent through an asymmetric Mach-Zehnder interferometer, formed by two optical path from two output ports, indexed as A and B. At each output port, photoevents are detected using single-photon avalanche detectors (APDs), which generate photodetection events. These events are time-stamped to extract interferometric photon correlations $g^{(2X)}(\tau)$ numerically. From the interferometric photon correlations at zero-time difference $g^{(2X)}(0)$, we extract the fraction ρ of coherent light.
BS: Beam splitter

correlation $1 \leq g^{(2)}_{\mathrm{unc}}(0) \leq 2$. This further constrains the possible solutions to ρ with an upper bound,

$$\rho \leq \sqrt{2 - 2\, g^{(2X)}_{\mathrm{mix}}(0)}, \tag{3.8}$$

and a lower bound,

$$\rho \geq \begin{cases} \frac{1}{2} + \frac{1}{2}\sqrt{3 - 4\, g^{(2X)}_{\mathrm{mix}}(0)}, & \text{for } \frac{1}{2} \leq g^{(2X)}(0) \leq \frac{3}{4} \\ 2 - 2\, g^{(2X)}_{\mathrm{mix}}(0), & \text{for } \frac{3}{4} \leq g^{(2X)}(0) \leq 1 \end{cases}, \tag{3.9}$$

with $g^{(2X)}_{\mathrm{mix}}(0)$ ranging from 1/2 for fully coherent light, to 1 for fully incoherent light.

3.2 Experimental configurations and methods

The experimental setup to extract the fraction ρ of coherent light is shown in Figure 3.2.

3.2.1 Equipment to measure $g^{(2X)}(\tau)$

- **Light source**

  We used a temperature-stabilised 780 nm distributed feedback semiconductor laser diode operating at different laser currents for the light source, The laser diode is free-running and not frequency-locked to any cavity or optically

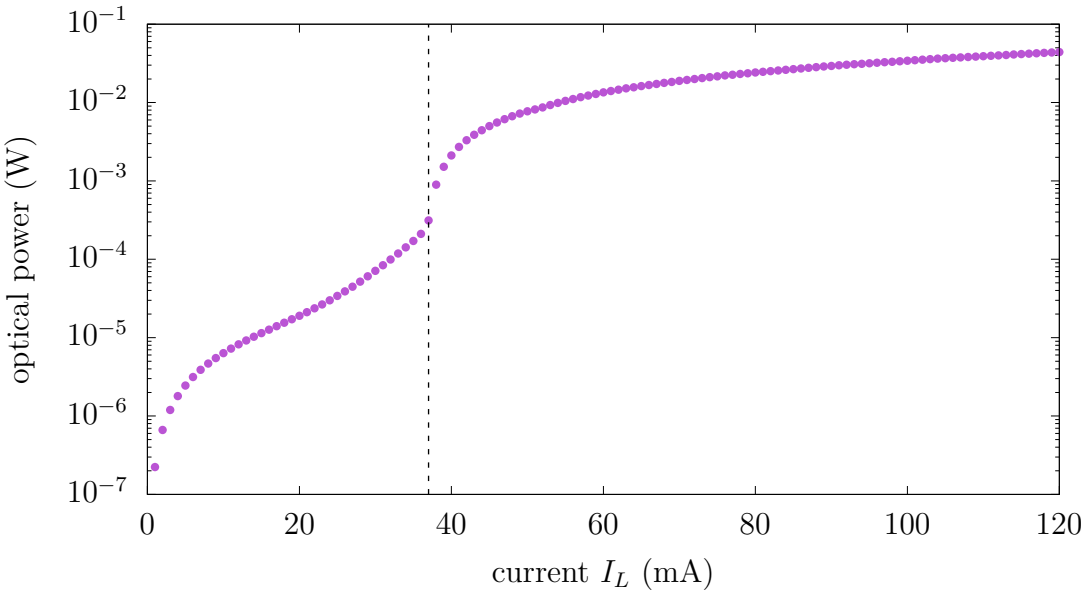

Figure 3.3: Measured optical power emitted by the laser at different laser currents I_L. The lasing threshold I_T is determined to be 37 mA (dotted lines), where the steepest increase in optical power was observed.

resonant medium. The frequency bandwidth for this diode is quoted to be 0.6...1 MHz.

For a first characterisation of the laser diode, we determined the lasing threshold by measuring the optical power emitted by the laser at different laser currents I_L from 1 to 120 mA in 1 mA steps shown in Fig 3.3. From this measurement, we identify the lasing threshold $I_T = 37$ mA at the laser current with the sharpest increase in optical power.

- **Beam splitters**

  For good spatial mode overlap, we used fused fibre couplers as the beam splitters in the asymmetric Mach-Zehnder interferometer. The fused fiber couplers are single-mode with a near 50:50 splitting ratio and has an operating range of 785±15 nm.

- **Propagation delay**

  We added an approximately 180 m long single-mode fibre in one arm of the interferometer which created a propagation delay Δ of about 900 ns. For a 780 nm laser with about 1 MHz bandwidth, the corresponding coherent time is

about 300 ns. The propagation delay of 900 ns delay is 3 times longer than the coherence time of the laser, sufficiently long enough for the delayed and non-delayed fields to be uncorrelated.

- **Single-photon detectors**
  Actively quenched silicon single-photon avalanche photodetectors with a timing resolution about 40 ps were used to detect photoevents at each output of the interferometer over an integration time of T. The photoevents were then timestamped using a time tagger with a 2 ns timing resolution. From the timestamps, we extract the interferometric photon correlation function $g^{(2X)}$ by computing each time difference τ between each pair of photoevents, with the number of pairs occurring for each time difference τ sorted into a histogram, which is then normalised using the integration time T. These measurements were repeated for different laser currents I_L, to extract the $g^{(2X)}(\tau)$ at each I_L.

3.2.2 Extracting parameters from $g^{(2X)}(\tau)$

To extract the fraction of coherent light ρ emitted by the laser diode, we determine $g^{(2X)}(0)$ from a fit of the interferometric photon correlation $g^{(2X)}(\tau)$. The negative component in the interferometric photon correlation $g^{(2X)}(\tau)$ is from the interferometric visibility $\|g^{(1)}(\tau)\|$ of the light source. As the interferometric visibility $\|g^{(1)}(\tau)\|$ of a light source is related to its spectral lineshape by a Fourier transform, we assumed the coherent light emitted by the laser has a Lorentzian lineshape [66], and hence model

$$g^{(2X)}(\tau) = 1 - A \cdot \exp\left(-\frac{2\,\|\tau\|}{\tau_c}\right), \tag{3.10}$$

where τ_c is the characteristic time constant of the coherent light, and A is the amplitude of the dip. we extract $g^{(2X)}(0)$ from the fit as $1-A$. Sample measurements of $g^{(2X)}(\tau)$ and their corresponding fits at laser current I_L below, near and above I_T are shown in Figure 3.4.

For easier computation of ρ from the Equation 3.10, we rewrite in terms of A following Equation 3.8 for the upper bound

$$\rho \leq \sqrt{2A}\,, \tag{3.11}$$

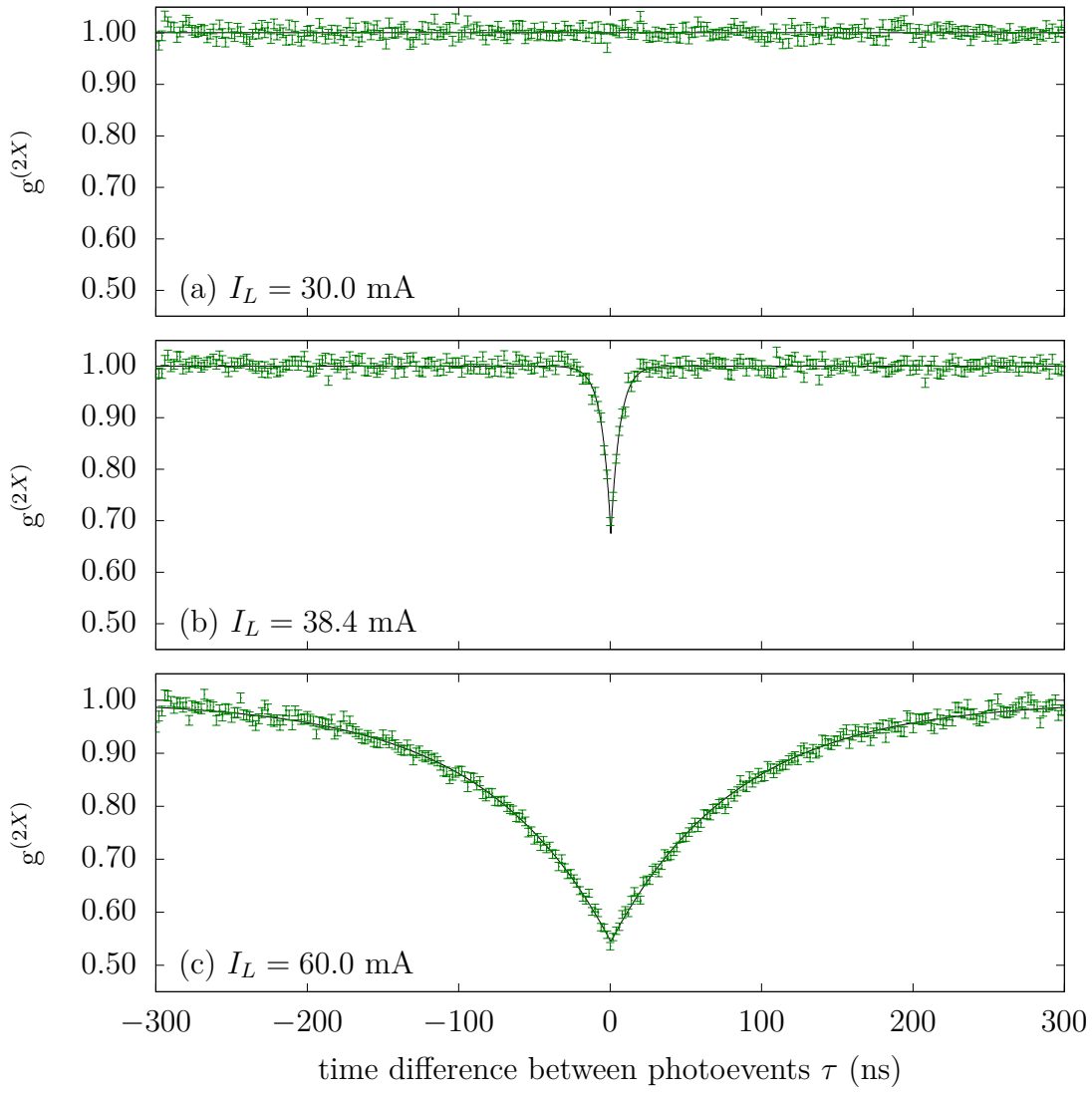

Figure 3.4: Measurements of interferometric photon correlations $g^{(2X)}(\tau)$ at different laser currents I_L relative to threshold current I_T: (a) $I_L = 30.0\,\text{mA}$ lesser than I_T, (b) $I_L = 38.0\,\text{mA}$ near I_T, and (c) $I_T = 60.0\,\text{mA}$ greater than I_T. The error bars at each time bin indicates an uncertainty expected from Poissonian counting statistics from the number of photoevent pairs with time difference matching the time bin. The black solid lines are fits to Equation 3.10, where A and coherence time τ_c is extracted. The fitted values of A are (a) -0.0006 ± 0.0003, (b) 0.29 ± 0.01 and (c) 0.455 ± 0.002. The fitted values of coherence time τ_c are (b) $7.9 \pm 0.4\,\text{ns}$ and (c) $168 \pm 1\,\text{ns}$.

and Equation 3.9 for the lower bound

$$\rho \geq \begin{cases} 2A, & \text{for } 0 \leq A \leq \frac{1}{4} \\ \frac{1}{2} + \frac{1}{2}\sqrt{4A-1}, & \text{for } \frac{1}{4} \leq A \leq \frac{1}{2} \end{cases} \tag{3.12}$$

3.2.3 Propagation of uncertainty from A to ρ

To obtain an uncertainty to the fraction ρ of coherent light, we require an error propagation from the variable A in Equation 3.11 and 3.12 the fraction ρ of coherent light. However, standard error propagation techniques do not apply here. For example, in applying standard error propagation techniques to Equation 3.12, the uncertainty σ_ρ of the fraction ρ of coherent light is related to A and its uncertainty via

$$\begin{aligned} \sigma_\rho =& \frac{\partial \rho}{\partial A}\sigma_A \\ =& \frac{\sigma_A}{\sqrt{2A}} \end{aligned} \tag{3.13}$$

where σ_A is the uncertainty of A obtained from fitting interferometric photon correlations $g^{(2X)}(\tau)$ to Equation 3.10.

We note that for values $A \approx 0$, this would lead to infinite uncertainties. Instead, we obtain ρ and its associated uncertainty σ_ρ by performing a variable transform on a probability distribution of A.

Instead of using standard error propagation techniques, we extract the uncertainty σ_ρ of the fraction of coherent light using a variable transform of probability distributions. We demonstrate this method to extract the lower bounds of fraction of coherent light ρ and its uncertainty σ_ρ from $A = 0.326 \pm 0.008$, extracted from the $g^{(2X)}(\tau)$ fit at $I_L = 38.0\,\text{mA}$. We first assume a normal probability distribution for the variable A

$$p_A(A) = \exp\left(-\frac{(A-\bar{A})^2}{2\sigma_A^2}\right) \tag{3.14}$$

with a mean at $\bar{A} = 0.326$ and a standard deviation $\sigma_A = 0.008$. Note that we ignore the scalar normalisation factor as we would renormalise the distribution to its area later.

We represent Equation 3.12 as a function f which maps the variable A to fraction of coherent light ρ. The transformed probability distribution to the variable ρ can

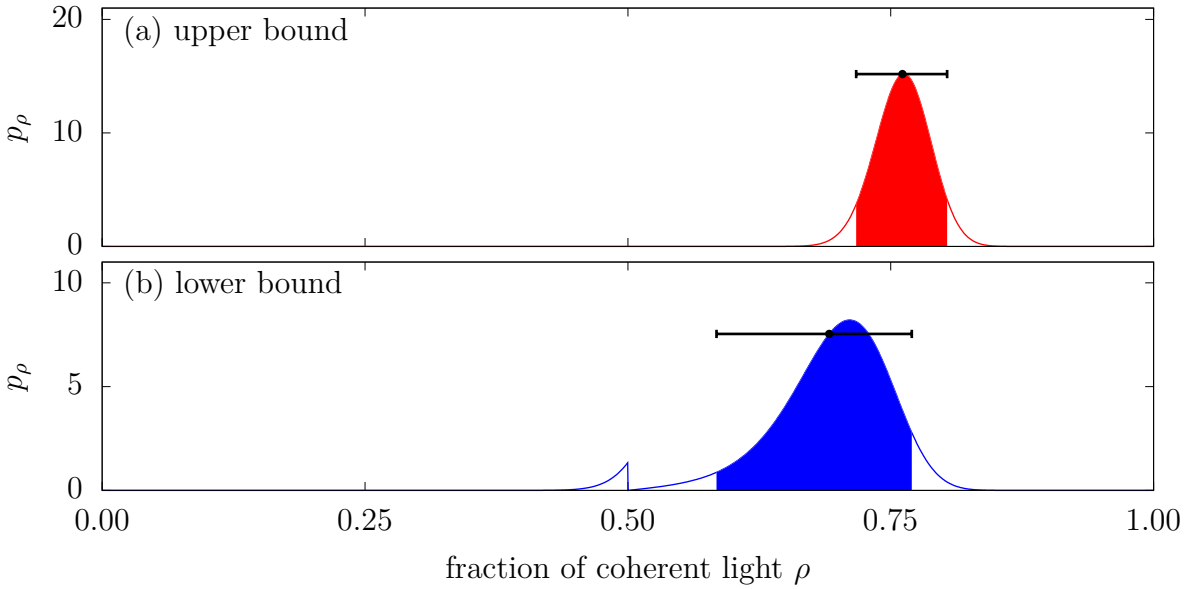

Figure 3.5: Probability distributions of the fraction ρ of coherent light (a) upper bound (red) and (b) lower bound (blue). The probability distributions were obtained from a variable transform of the probability distribution of A in Equation 3.10, extracted from interferometric photon correlations $g^{(2X)}(\tau)$ measured at a laser current $I_L = 38.0\,\text{mA}$. The shaded areas covers the 5^{th} to 95^{th} percentile of the probability distribution, which contains a 90% confidence interval for ρ. The black points indicate the mean value of ρ for each of the respective bounds, with the error bars demarcating the 5^{th} and 95^{th} percentiles.

be written as

$$\begin{aligned} p_\rho(\rho) &= p_A(f^{-1}(\rho)) \cdot \frac{d}{d\rho}(f^{-1}(\rho)) \\ &= \begin{cases} \frac{1}{2}\exp\left(-\frac{\left(\frac{\rho}{2}-\bar{A}\right)^2}{2\sigma_A^2}\right) & \text{for } 0 \le \rho \le \frac{1}{2} \\ (2\rho-1)\exp\left(-\frac{(\frac{(2\rho-1)^2+1}{4}-\bar{A})^2}{2\sigma_A^2}\right) & \text{for } \frac{1}{2} \le \rho \le 1 \\ 0 & \text{otherwise} \end{cases} \end{aligned} \tag{3.15}$$

We normalise the distribution $p_\rho(\rho)$ numerically by dividing its area under the curve, producing a normalised probability distribution, as shown in Figure 3.5(b). Using this normalised probability distribution, we find the mean value of ρ and error bars, which we define as a confidence interval between the 5th percentile and 95th percentile of the probability distribution, covering 90% of the distribution in this interval.

3.2.4 Transition from incoherent to coherent light

Using the setup shown in Figure3.2, we extracted the interferometric photon correlations $g^{(2X)}(\tau)$ at different laser currents I_L as shown in Figure 3.6(a). From these $g^{(2X)}(\tau)$, we extracted the the expectation values and confidence intervals for the upper and lower bounds fraction of coherent light ρ, as shown in Figure 3.6, middle.

From our measurements, the fraction of coherent light ρ remains near 0 below the lasing threshold. Above this threshold, ρ increases quickly with the laser current I_L, appearing like a phase-transition from incoherent to coherent light. Both the upper and lower bounds for the fraction of coherent light reached a mean value of $\rho = 0.986$, within a 90% confidence interval 0.982 to 0.989, at $I_L = 120\,\text{mA}$. The result agrees with the expectation that, as the laser current is increased above the lasing threshold, the laser diode dominantly generates coherent light from stimulated emission.

From Figure 3.6, middle, we can also see that the extracted upper bounds and lower bounds are quite close together, even at laser currents near the lasing threshold. This suggests that the heuristic model of the mixture light field in Equation 3.1, describes the nature of light well even through the phase transition from incoherent to coherent emission.

We also extracted the characteristic time constant τ_c at each I_L from the fit of $g^{(2X)}(\tau)$ to Equation 3.10, as shown in Figure 3.6, bottom. We observe an increase in τ_c with the laser current after the threshold current, before reaching a steady coherence time τ_c between 300 ns and 350 ns, around laser current $I_L = 100$ to 120 mA.

The coherence time τ_c of the coherent light field E_{coh} is related to the frequency full-width at half-maximum bandwidth Δf via

$$\Delta f = \frac{1}{\pi \tau_c}. \tag{3.16}$$

Using Equation 3.16, the coherence time τ_c observed of about 300 ns around laser current $I_L = 100$ to 120 mA, translates to a bandwidth $\Delta f \approx 1\,\text{MHz}$. This increase in the coherence time τ_c corresponds to a narrowing of the emission linewidth. This is in agreement with predictions from laser theory which expects a line narrowing

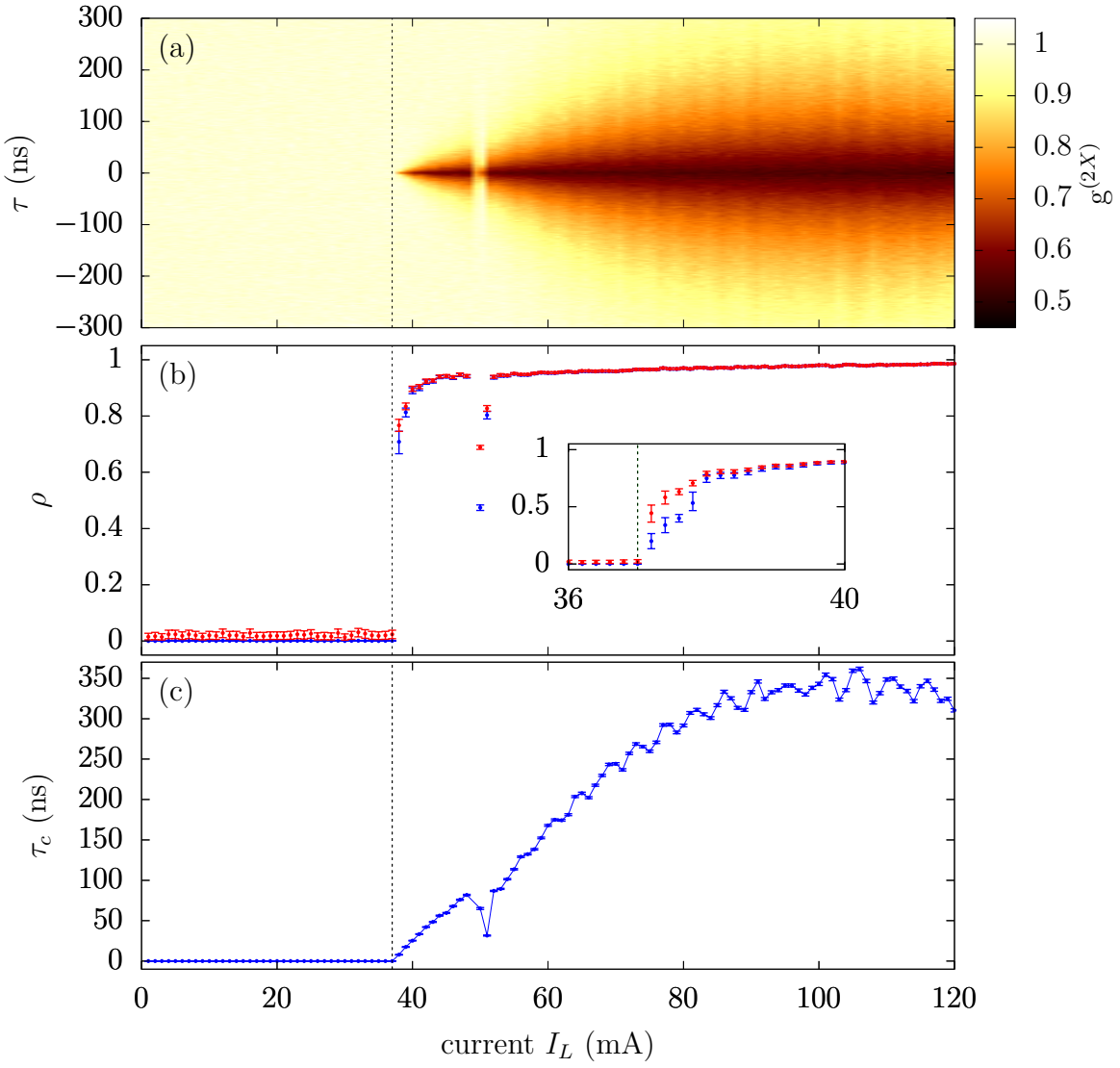

Figure 3.6: (a) Interferometric photon correlations $g^{(2X)}(\tau)$ measured for different laser currents I_L. (b) Fraction ρ of coherent light ρ upper bounds (red) and lower bounds (blue) from fitting interferometric photon correlations $g^{(2X)}(\tau)$ to Equation 3.10. The expectation values and the error bars shown are propagated from the uncertainty of A from the fit using the methods described in Section 3.2.3. The inset shows the mean value and bounds for fraction ρ of coherent light in finer laser current steps near the threshold current. (c) Coherence time τ_c extracted from fitting interferometric photon correlations $g^{(2X)}(\tau)$ to Equation 3.10. The vertical dashed lines indicate the threshold current $I_T = 37$mA.

with increasing pump power [67]. We also observed a small modulation of this characteristic timescale for larger laser currents, with a periodicity of about 6 mA.

3.2.5 Transition across a mode-hop

As shown in Figure 3.6, we observe a reduction in the fraction of coherent light ρ between the laser current range of 49 to 51 mA. We also observe a reduction in the characteristic time constant τ_c in the same laser current range.

Upon this observation, our hypothesis is a longitiudinal laser mode-hop occurring in this laser current range. A laser mode-hop occurs when the emitters in the laser can be resonant with different longitudinal modes when operating above the lasing threshold. This results in a competition of coherent emission into different frequencies, or a multimode operation

To further check if a mode-hop occurs between 49 to 51 mA, we measured the spectrum of light emitted by the laser diode in this laser current range with an optical spectrum analyser with a spectral resolution of 2 GHz (Bristol 771B-NIR). In this current range, the laser diode indeed emitted light into two distinct spectral bands, centered around 780.07 nm and 780.34 nm, as shown in Figure 3.7(a) and (b). Thus, a mode hop is a very likely cause for this behaviour. For a better comparison of the spectrum at different currents, we divided the spectral intensity at each wavelength bin by the power in the wavelength range of 779.9 nm to 781.0 nm to normalise the spectral intensity.

To extract a ratio of power emitted between the two spectral bands, we assumed the two bands have the same spectral lineshape and spectral linewidth, with the optical power emitted in each band proportional to its peak spectral intensity. Using these assumptions, we quantified the power ratio

$$r_{\alpha,\beta} = \frac{P_{\alpha,\beta}}{P_\alpha + P_\beta}\,, \tag{3.17}$$

where α, β indexes the spectral bands centered around 780.07 nm and 780.34 nm, respectively, and $P_{\alpha,\beta}$ is the peak spectral intensity in the respective bands. We extract $r_{\alpha,\beta}$ from the measured spectrum at different currents as shown in Figure 3.7(c). We observe a nearly linear transition of the power ratios across the region of mode hop between $I_L = 49$ mA and 52 mA.

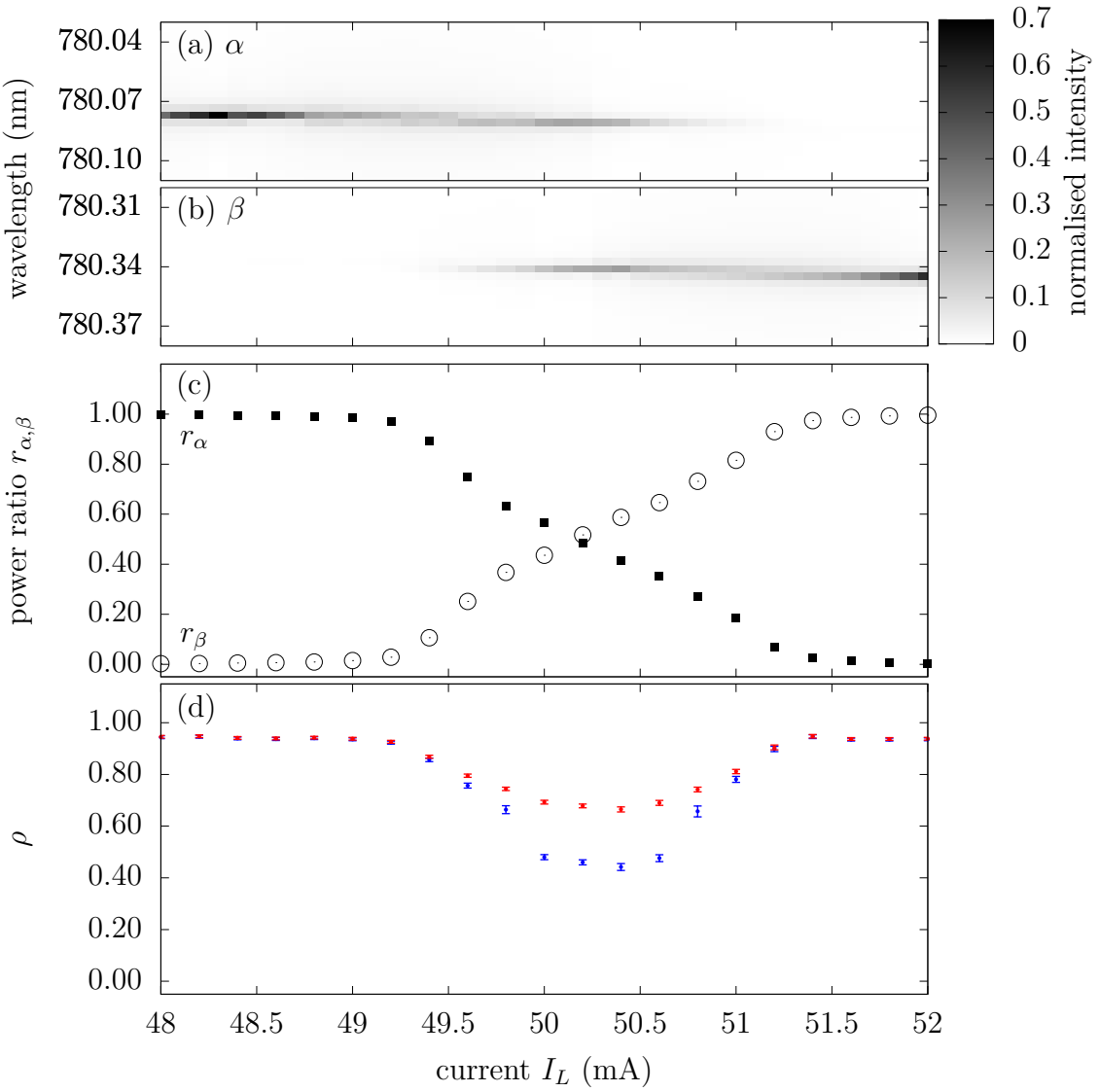

Figure 3.7: Different longitiudinal "chip" modes of the laser diode were excited at different currents, and mode-hop was observed. The mode-hop resulted in a reduction in fraction of coherent light ρ. The spectrum of light emitted from laser diode in the two distinct frequency bands as shown in (a) a frequency band centered around 780.07 nm and (b) a frequency band centered around 780.34 nm, indexed as α and β respectively. (c) Power ratio $r_{\alpha,\beta}$ of light emitted into the respective spectral band α around 780.07 nm (solid squares) and β at 780.34 nm (open circles), respectively at different currents . (d) Upper bounds (red) and lower bounds (blue) for the fraction ρ of coherent light extracted from interferometric photon correlations $g^{(2X)}(\tau)$ using the methods described in Section 3.2.3.

We also measured interferometric photon correlations $g^{(2X)}(\tau)$ from $I_L = 49\,\mathrm{mA}$ to $52\,\mathrm{mA}$ and extracted the fraction ρ of coherent light, as shown in Figure 3.7(d). Across this current range, we observed a reduction of ρ with its lowest value between $50.0\,\mathrm{mA}$ to $50.2\,\mathrm{mA}$. In this current range, the two modes have a similar power fraction $r_\alpha \approx r_\beta$. We interpret this reduction in the fraction of coherent light as these different modes being incoherent to each other, although each mode may be coherent to itself, resulting in the light emitted to be a mixture of a coherent mode, and an uncorrelated mode.

Summary

We have presented a technique to quantify the fraction of coherent light ρ emitted by a laser diode using interferometric photon correlations $g^{(2X)}$. To do this, we modelled this mixture of light as a superposition of a coherent light in a single mode with another light in uncorrelated mode. From this model, we established a relationship between interferometric photon correlations $g^{(2X)}(\tau)$, and upper and lower bounds for the fraction ρ of coherent light, which required a non-standard numerical method of error propagation. In our experiments, we measured ρ as the light emitted by the laser diode, changing from incoherent to dominantly coherent light across the lasing threshold in a phase transition-like manner. We recorded a maximum fraction of coherent light $\rho = 0.986$ within a 90% confidence interval of 0.982 to 0.986, with a spectral bandwidth of about $1\,\mathrm{MHz}$. Using this technique, we have also identified a range of laser currents above the lasing threshold where a reduction in the fraction ρ of coherent light was observed. We measured the spectrum of light emitted in this range of currents and found emission in two spectral bands, suggesting a mode competition between two longitudinal modes. From this, we interpreted the reduction of coherent light fraction as a result of the two longitudinal modes being uncorrelated to each other although each mode may be coherent to itself.

Chapter 4

Mechanisms of photon bunching

Photon bunching can result from various mechanisms. One such mechanism involves amplitude modulation of the entire light field, such as from inherent intensity noise of the source [1] or via intensity modulators [47, 68]. Another mechanism is the superposition of phase-randomised light fields, like the light emitted from gas discharge lamps, which models light with statistical properties similar to blackbody radiation, referred to as thermal light [12, 69]. This mechanism also underpins light scattered off particles [15–17] and rotating ground glass plates [18–20, 22, 23], which are commonly regarded as techniques to generate light with properties similar to thermal light.

Identifying the mechanism for photon bunching is crucial to determine the source of randomness causing the effect. Although photon bunching can be observed as a peak in the second-order photon correlation $g^{(2)}(\tau)$, typically measured with a Hanbury-Brown and Twiss type experiment, the information provided, such as the timescale and amplitude of the photon bunching, may be insufficient to deduce the specific mechanisms causing the photon bunching. This motivates the need for complementary techniques to identify these mechanisms.

In this Chapter, we use interferometric photon correlation $g^{(2X)}(\tau)$ to infer the mechanism causing the photon bunching in bunched light. This technique is an adaptation from Lebreton et al. [2], who used this to distinguish a light source producing amplified spontaneous emission from a laser with intensity noise. Here, we use this technique on two bunched light sources commonly substituted for a blackbody radiator: laser light scattered off a rotating ground glass plate, and green emission lines from a mercury discharge lamp around 546 nm.

We found the second-order photon correlation $g^{(2)}(\tau)$ of laser light scattered off a rotating ground glass plate occurs on timescale and temporal profile different from its interferometric visibility $\|g^{(1)}(\tau)\|$. This suggests that the photon bunching mechanism cannot be purely due to phase fluctuations. In contrast, the emission line from a mercury discharge lamp shows an interferometric photon correlation $g^{(2X)}(\tau)$ indicating that the temporal profile and timescale of second-order photon correlation $g^{(2)}(\tau)$ and interferometric visibility-square $\|g^{(1)}(\tau)\|^2$ are identical, implying that the photon bunching is related to the phase fluctuations. Furthermore, the interferometric photon correlations $g^{(2X)}(\tau)$ of the mercury discharge lamp shows that Siegert relation is obeyed, suggesting that it emits thermal light.

4.1 Thermal light and the Siegert relation

An example of light that exhibit photon bunching caused by phase fluctuations is thermal light. To understand how phase fluctuations can result in photon bunching, we show how a thermal light's interferometric visibility $\|g^{(1)}(\tau)\|$, which characterises the phase fluctuation in a light source, is connected to its second-order photon correlation $g^{(2)}(\tau)$. This connection is often referred to as the Siegert relation [65]. Here we present a derivation of the Siegert relation adapted from Loudon [5].

Thermal light is commonly modelled as a superposition of the individual light fields from independently phased emitters $E_j(t)$ in an ensemble

$$E(t) = \sum_{j=1}^{N} \frac{1}{\sqrt{N}} E_j(t), \tag{4.1}$$

where N is the number of emitters in the ensemble. For simplicity, we have adopted a normalisation such that $\|E(t)\| = \|E_j(t)\| = 1$. The independent phasing between fields of different indices satisfies the condition

$$\langle E_j^*(t) E_k(t+\tau) \rangle = 0 \text{ for } j \neq k\,. \tag{4.2}$$

An assumption commonly made for thermal light is that the first-order field correlations $g^1(\tau)$ between emitters and with the ensemble are identical:

$$g^{(1)}(\tau) = \frac{\langle E^*(t) E^*(t+\tau) \rangle}{\langle E(t) E(t) \rangle} = \frac{\langle E_j^*(t) E_j(t+\tau) \rangle}{\langle E_j^*(t) E_j(t) \rangle}. \tag{4.3}$$

Using Equation 4.1, the second-order photon correlation of thermal light is

$$\begin{aligned} g^{(2)}(\tau) =& \frac{\langle E^*(t)E^*(t+\tau)E(t+\tau)E(t)\rangle}{\langle E^*(t)E(t)\rangle\langle E^*(t)E(t)\rangle} \\ =& \frac{1}{N^2}\sum^{j,k,l,m}\langle E_j^*(t)E_k^*(t+\tau)E_l(t+\tau)E_m(t)\rangle\,. \end{aligned} \tag{4.4}$$

Therein, terms that contain an unequal number of E and E^* with the same index„ such as $\langle E_j^*(t)E_j^*(t+\tau)E_j(t+\tau)E_k(t)\rangle$, vanish. The remaining non-zero terms are $j=k=l=m$:

$$\sum^{j}\langle E_j^*(t)E_j^*(t+\tau)E_j(t+\tau)E_j(t)\rangle = N, \tag{4.5}$$

$j=l, k=m$:

$$\begin{aligned} &\sum^{j\neq k}\langle E_j^*(t)E_k^*(t+\tau)E_k(t+\tau)E_j(t)\rangle \\ =&\sum^{j\neq k}\langle E_j^*(t)E_j(t)\rangle\langle E_k^*(t)E_k(t)\rangle \\ =&N(N-1), \end{aligned} \tag{4.6}$$

$j=m, k=l$:

$$\begin{aligned} &\sum^{j\neq k}\langle E_j^*(t)E_k^*(t+\tau)E_j(t+\tau)E_k(t)\rangle \\ =&\sum^{j\neq k}\langle E_j^*(t)E_j(t+\tau)\rangle\langle E_k^*(t+\tau)E_k(t)\rangle \\ =&N(N-1)\left\|g^{(1)}(\tau)\right\|^2, \end{aligned} \tag{4.7}$$

We sum the terms in Equation 4.5 to 4.7, which leads to the Siegert relation

$$\begin{aligned} g^{(2)}(\tau) =& \frac{1}{N^2}\left[N+N(N-1)+N(N-1)\left\|g^{(1)}(\tau)\right\|^2\right] \\ =& 1+\left(1-\frac{1}{N}\right)\left\|g^{(1)}(\tau)\right\|^2 \\ \approx& 1+\left\|g^{(1)}(\tau)\right\|^2, \end{aligned} \tag{4.8}$$

where $1/N \to 0$ assuming a large number N. We note that the interferometric visibility $\|g^{(1)}(\tau)\|$ in Equation 4.8 refers to the interferometric visibility of the individual emitters, which has been assumed to be identical to the ensemble.

4.2 Experimental settings

In this Section, we describe our preparation of two bunched light sources: light from a mercury discharge lamp and light scattered off a rotating ground glass plate

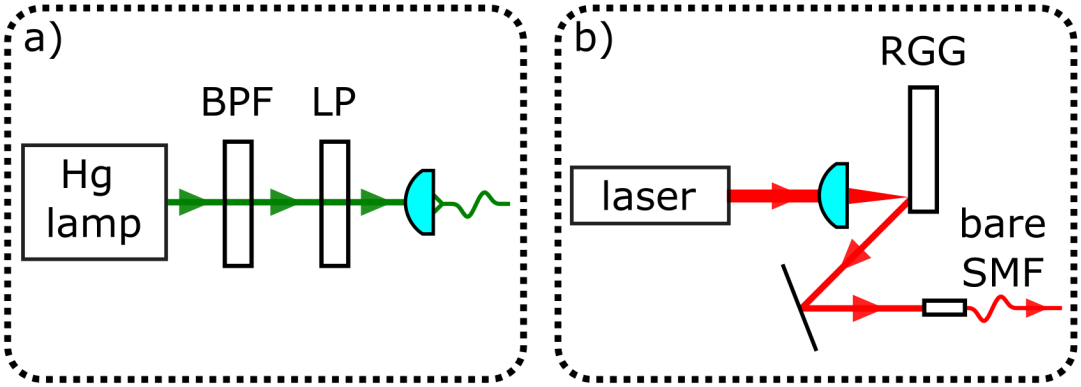

Figure 4.1: Setup for different bunched light sources. (a) Mercury discharge lamp. Light from the lamp is filtered with a 546 nm bandpass filter (BPF) and a linear polariser (LP). With an aspheric lens, some of the light is focused into a multimode fibre before projecting into a single mode fibre. (b) Laser light scattered off a rotating reflective ground glass plate. Light from a 780 nm laser is focused onto a rotating ground glass plate. Laser light scattered off the ground glass plate is sampled directly into a single mode fibre (SMF) 19 cm away.

illuminated by a laser. We also describe the setups to extract second-order photon correlations $g^{(2)}(\tau)$ and interferometric photon correlations $g^{(2X)}(\tau)$ for the respective light sources.

Mercury discharge lamp

The setup to prepare the light emitted from a mercury discharge lamp is shown in Figure 4.1(a). The emission of mercury is filtered with an optical bandpass with a center wavelength of 546 nm and a bandwidth of 3 nm. A single polarisation is selected using a linear polariser with an extinction ratio of about $1000:1$ between two orthogonal linear polarisations. The filtered light is then sampled by focusing some of the light into a multimode fibre. The light from the multimode fibre is then projected into a single spatial mode as it enters a single-mode fused fibre coupler, which forms part of a Hanbury-Brown and Twiss setup to measure second-order photon correlations $g^{(2)}(\tau)$, as shown in Figure 2.2(a), or as part of the asymmetric Mach-Zehnder interferometer to extract the interferometric photon correlations $g^{(2X)}(\tau)$.

For the asymmetric Mach-Zehnder interferometer, we used a single mode fibre

about 2 m long to create a propagation delay of about 10 ns between the two paths of the interferometer. We used actively quenched silicon avalanche photodetectors with a 40 ps timing jitter to detect photoevents for both second-order photon correlations $g^{(2)}(\tau)$ and interferometric photon correlations $g^{(2X)}(\tau)$ measurements. The photoevents were logged using a timestamp card with a timing resolution of about 4 ps.

Laser light scattered off rotating ground glass plate

To prepare this light source, we used a distributed feedback laser emitting light with central wavelength at 780 nm. The laser is focused on a reflective ground glass plate diffuser with a grit of 1500, with an estimated beam diameter W on the ground glass plate of about 4 μm, at a radial distance R of about 10 mm off-centred from the rotation axis of the ground glass plate. A rotation motor coaxial to centre of the ground glass plate rotates the ground glass plate with a period T_0 of about 4 ms. A single mode fibre for 780 nm was placed 19 cm away from the illuminated spot to sample some of the scattered light into a single spatial mode.

To extract interferometric photon correlations $g^{(2X)}(\tau)$, the sampled light is sent through an asymmetric Mach-Zehnder interferometer similar to the setup in Figure 2.1. In the interferometer, we used fused fibre couplers compatible with 780 nm light as beamsplitters, and a single mode fibre of about 400 m long, to create a propagation delay Δ of about 2 μs between the two paths of the inteferometer. Actively quenched silicon avalanche photodiodes with a timing jitter of 40 ps were used to detect photoevents. The detection timing of photoevents were logged with a timestamp card with 2 ns resolution. To extract second-order photon correlation $g^{(2)}(\tau)$, one path of the interferometer was obstructed, which created a Hanbury-Brown Twiss type interferometer with the remaining components of the setup, as shown in Figure 2.2(b).

As a characterisation of the laser light, we extracted the interferometric photon correlations $g^{(2X)}(\tau)$, without the rotating ground glass plate as shown in Figure 4.2. Using the techniques in Chapter 3, we find that it has a coherence time $\tau_c = 200 \pm 1$ ns, and a dip amplitude $A = 0.456 \pm 0.002$, which translates to fraction of coherent light emitted by the laser $\rho = 0.954$ with a 90% confidence interval between 0.950

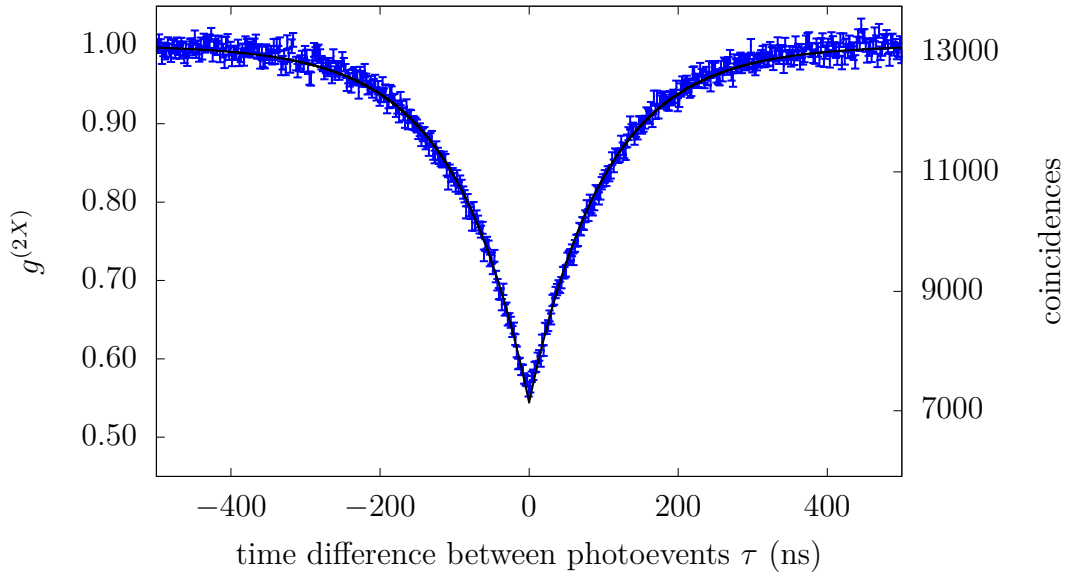

Figure 4.2: Interferometric photon correlation $g^{(2X)}(\tau)$ for the laser light before scattering off the rotating ground glass plate. Blue points show the measured data and black solid lines show the fitted curves to Equation 3.10, from which we extracted a coherence time $\tau_c = 200 \pm 1\,\text{ns}$ and a dip amplitude $A = 0.456 \pm 0.002$. Using the techniques presented in Chapter 3, the dip amplitude translates to a fraction of coherent light emitted by the laser to be $\rho = 0.954$ with a 90% confidence interval between 0.950 to 0.958.

to 0.958.

4.3 Photon bunching in both sources

To analyse the photon bunching phenomena in these two sources, we present suitable models for the second-order photon correlations $g^{(2)}(\tau)$ for these two light sources. We then fit the second-order photon correlations $g^{(2)}(\tau)$ extracted from measurement to these models to extact characteristic timescales and amplitude of the photon bunching.

Mercury discharge lamp

The green emission lines of the mercury discharge lamp around 546 nm are contributed by different isotopes and hyperfine transition of mercury, with different intensities [70]. In the discharge lamp, each of these emission lines are expected to

be Doppler broadened by the temperature of the lamp at about 400 K, which results in a Gaussian spectral profile in each of the emission lines. However, these Doppler broadened emission lines have spectral overlaps which results in a complex spectrum of the emission around 546 nm. Nevertheless, we approximate the spectrum to have a Gaussian profile. From the Wiener-Khintchine [63, 64] theorem, which relates the spectrum of a signal to its autocorrelation function by a Fourier transform, this Gaussian spectral profile implies that the second-order photon correlation of the light from the mercury discharge lamp also has a Gaussian profile

$$g^{(2)}(\tau) = 1 + \beta_{\mathrm{Hg}} \cdot \exp\left[-\left(\frac{\tau}{\tau_{\mathrm{Hg}}}\right)^2\right], \tag{4.9}$$

where β_{Hg} is the amplitude of the bunching peak, and τ_{Hg} is the characteristic timescale of this bunching feature.

We fitted the measured second-order photon correlation $g^{(2)}(\tau)$ for light from the mercury discharge lamp to Equation 4.9, shown in Figure 4.3(a). From the fit, we extracted $\beta_{\mathrm{Hg}} = 0.144 \pm 0.009$, $\tau_{\mathrm{Hg}} = 0.23 \pm 0.02$ ns, and a reduced-$\chi^2 = 2.80$.

Laser light scattered off rotating ground glass plate

For the laser light scattered off the rotating ground glass plate, we expected a Gaussian profile for its second-order photon correlations $g^{(2)}(\tau)$ from theoretical models of light diffracting from the ground glass plate [20, 22, 71, 72]

$$g^{(2)}(\tau) = 1 + \beta_{\mathrm{RGG}} \cdot \exp\left[-\left(\frac{\tau}{\tau_{\mathrm{RGG}}}\right)^2\right], \tag{4.10}$$

where β_{RGG} is the amplitude of the bunching peak, and τ_{RGG} is the characteristic timescale of this bunching feature.

From these models, we can predict τ_{RGG} for a beam focused on the ground glass plate with the light scattered from the ground glass plate collected at distance significantly longer than the beam diameter on the ground glass plate

$$\tau_{\mathrm{RGG}} \approx \frac{WT_0}{4\pi R}, \tag{4.11}$$

where T_0 is the period of rotation of the ground glass plate, W is the beam diameter on the ground glass plate and R is the radial distance of the beam spot on the

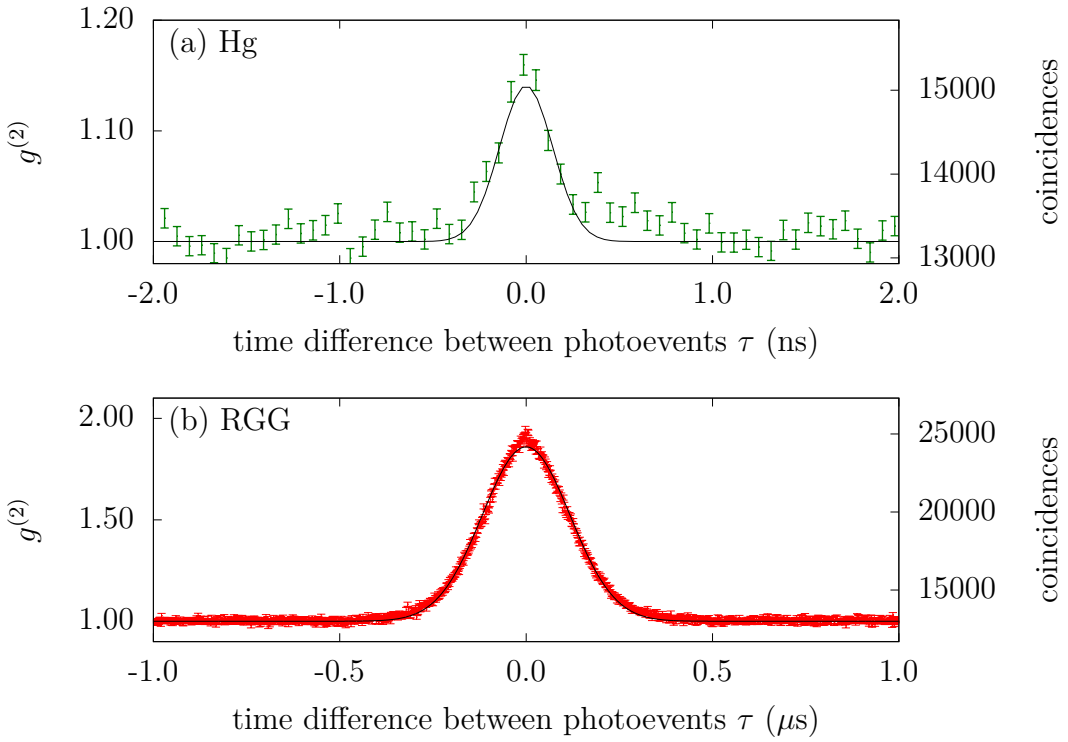

Figure 4.3: Second-order photon correlations $g^{(2)}(\tau)$ for (a) mercury discharge lamp (green) and (b) laser light scattered off a rotating ground glass plate (red). Solid lines show the fitted curves to Equation 4.9 for mercury discharge lamp and Equation 4.10. From the fit, we extract the photon bunching amplitude $\beta_{\mathrm{Hg}} = 0.144 \pm 0.009$ and a characteristic timescale $\tau_{\mathrm{Hg}} = 0.23 \pm 0.02\,\mathrm{ns}$ for the mercury discharge lamp, a photon bunching amplitude $\beta_{\mathrm{RGG}} = 0.858 \pm 0.002$ and a characteristic timescale $\tau_{\mathrm{RGG}} = 167.1 \pm 0.3\,\mathrm{ns}$ for the laser light scattered off the rotating ground glass plate.

ground glass plate from the axis of rotation. Using Equation 4.11, we predict $\tau_{\mathrm{RGG}} = 130 \pm 30\,\mathrm{ns}$ based on our experimental settings.

We fitted the measured $g^{(2)}(\tau)$ for the laser light scattered off the rotating ground glass plate to Equation 4.10, shown in Figure 4.4(b). From the fit, we extract $\beta_{\mathrm{RGG}} = 0.858 \pm 0.002$, $\tau_{\mathrm{RGG}} = 167.1 \pm 0.3\,\mathrm{ns}$, and a reduced-$\chi^2 = 1.18$. The extracted value of $\tau_{\mathrm{RGG}} = 167\,\mathrm{ns}$ is close to predicted value of $130 \pm 30\,\mathrm{ns}$ from experimental settings using Equation 4.11, with the difference attributed to accumulated errors in measuring beam diameter W, rotation period T_0 of the ground glass plate and radial distance R of the beam spot on the ground glass plate from the rotation axis.

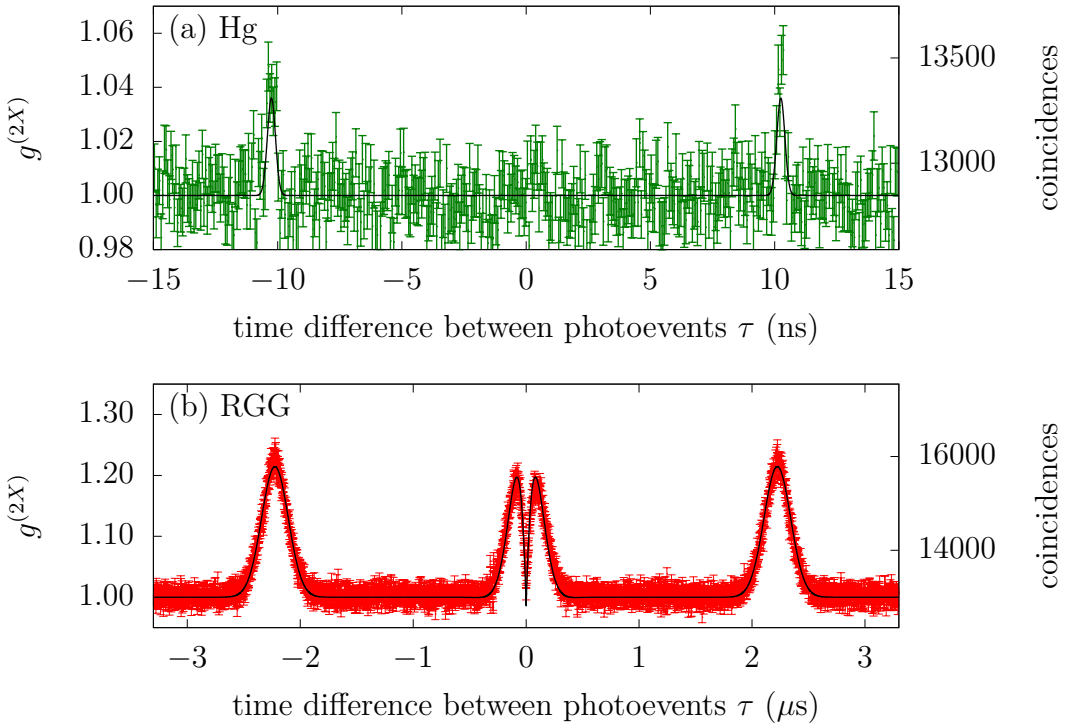

Figure 4.4: Interferometric photon correlations $g^{(2X)}(\tau)$ of (a) mercury discharge lamp (green) (b) laser light scattered off a rotating ground glass plate. Solid lines show the fitted curves to (a) Equation 4.12 and (b) Equation 4.10 for the interferometric photon correlations $g^{(2X)}(\tau)$ extracted from measurements.

4.4 Distinct photon bunching mechanisms

To determine if the photon bunching of these two light sources are related to their respective phase fluctuations, we extract their interferometric photon correlations $g^{(2X)}(\tau)$, as shown in Figure 4.4. We observe the features around zero-time difference in the interferometric photon correlations $g^{(2X)}(\tau \approx 0)$, to compare the residual difference between second-order photon correlations and interferometric visibility $g^{(2)}(\tau) - \|g^{(1)}(\tau)\|^2$. If the residual difference follows a unimodal distribution the photon bunching may be related to the phase fluctuation. Otherwise, if the residual difference follows a multimodal distribution, the photon bunching may be caused by other mechanisms rather than phase fluctuations.

Mercury discharge lamp

For the emission from the mercury discharge lamp, its interferometric photon correlation $g^{(2X)}(\tau)$ around zero-time difference appears constant at $g^{(2X)}(\tau \approx 0) = 1$, obeying Siegert relation which suggests it may be a thermal light source. Obeying the Siegert relation would further suggest that the photon bunching of this light source is related to its phase fluctuations.

Using Equation 2.9, which describes the interferometric photon correlation $g^{(2X)}(\tau)$ for a thermal light source, and the second-order photon correlation $g^{(2)}(\tau)$ of the emission from the mercury discharge lamp in Equation 4.9, its interferometric photon correlation is

$$g^{(2X)}(\tau) = 1 + \frac{\beta_{\mathrm{Hg}}}{4}\left[\exp\left(-\left\|\frac{2(\tau+\Delta)}{\tau_{\mathrm{Hg}}}\right\|\right) + \exp\left(-\left\|\frac{2(\tau-\Delta)}{\tau_{\mathrm{Hg}}}\right\|\right)\right], \tag{4.12}$$

where β_{Hg} is the photon bunching amplitude, τ_{Hg} is the characteristic timescale of the photon bunching, and Δ is propagation delay in the asymmetric Mach-Zehnder interferometer.

We fitted the extracted interferometric photon correlation $g^{(2X)}(\tau)$ using Equation 4.12, with the propagation delay Δ the only free parameter in the fit. The other parameters were obtained from fitting the second-order photon correlation $g^{(2)}(\tau)$ of the emission line from the mercury discharge lamp to Equation 4.9 in the previous Section. The fitted interferometric photon correlation $g^{(2X)}(\tau)$ is shown as a solid line in Figure 4.4(a). The fit has a reduced-$\chi^2 = 1.10$ for the $g^{(2X)}(\tau)$ measured with mercury discharge lamp, a value close to 1 which suggests that it conforms well to the model for thermal light.

Laser light scattered off a rotating ground glass plate

The interferometric photon correlations $g^{(2X)}(\tau)$ for the laser light scattered off a rotating ground glass plate is shown in Figure 4.4b. We observed that interferometric photon correlations $g^{(2X)}(\tau)$ around zero-time difference $\tau \approx 0$ seems to feature a bimodal distribution; the presence of both a peak and a dip feature on different characteristic timescales, with both features centered around $\tau \approx 0$. The bimodal distribution suggests that the photon bunching is not purely due to the phase fluctuations.

From Equation 2.9, the peaks observed in Figure 4.4b are related to the photon bunching. We interpret this as primarily due to amplitude modulation of the laser light by the rotating ground glass plate. On the other hand, the dip feature is related to the phase fluctuations of the light field, which we attribute to phase fluctuations of the laser. We thus modelled the second-order photon correlation $g^{(2)}(\tau)$ as following the model of laser light scattered off a rotating ground glass plate in Equation 4.10, and interferometric visiblity $\|g^{(1)}(\tau)\|$ as having a two-sided exponential decay, assuming the spectrum of the laser has a Lorentzian lineshape. This results in the interferometric photon correlation

$$\begin{aligned} g^{(2X)}(\tau) =& 1 + \frac{\beta_{\mathrm{RGG}}}{4}\left[\exp\left[-\left(\frac{\tau-\Delta}{\tau_{\mathrm{RGG}}}\right)^2\right] + \exp\left[-\left(\frac{\tau+\Delta}{\tau_{\mathrm{RGG}}}\right)^2\right]\right] \\ &+ \frac{1}{2}\left[\beta_{\mathrm{RGG}}\cdot\exp\left[-\left(\frac{\tau}{\tau_{\mathrm{RGG}}}\right)^2\right] - A\cdot\exp\left(-\left\|\frac{2\tau}{\tau_c}\right\|\right)\right], \end{aligned} \tag{4.13}$$

where β_{RGG} is the photon bunching amplitude, τ_{RGG} is the characteristic timescale of the photon bunching, τ_c is the coherence time of the laser light, A is the amplitude of the dip, and Δ is the propagation delay in the asymmetric Mach-Zehnder interferometer.

We fitted the extracted interferometric photon correlation $g^{(2X)}(\tau)$ using Equation 4.13 with the propagation delay Δ, the coherence time τ_c of the laser light, the amplitude A of the dip as free parameters for the fit. For the other parameters such as the photon bunching amplitude β_{RGG} and characteristic timescale of photon bunching τ_{RGG}, we use parameters extracted from fitting the second-order photon correlations $g^{(2)}(\tau)$ to Equation 4.10 in the previous section. From the fit, we extract the laser light's coherence time $\tau_c = 141 \pm 1\,\mathrm{ns}$, and a dip amplitude $A = 0.445 \pm 0.003$. The dip amplitude, suggests a fraction of coherent light about $\rho = 0.942$, with a 90% confidence interval between 0.935 to 0.949. The fit has a reduced-$\chi^2 = 1.20$, suggesting a good fit to the model provided in Equation 4.13.

In comparison to the interferometric photon correlation $g^{(2X)}(\tau)$ extracted from the laser source without the ground glass plate, we observe a reduction of the laser light's coherence time from $\tau_c = 200 \pm 1\,\mathrm{ns}$ to $\tau_c = 141 \pm 1\,\mathrm{ns}$, and a reduction of the mean fraction of coherent light from $\rho = 0.954$ to 0.942. The reduction in coherence time τ_c and mean fraction of coherent light ρ may be attributed to some random phase modulation of the laser light by multiple scattering sites on the rotating

ground glass plate. Nevertheless, the second-order photon correlation $g^{(2)}(\tau)$ and interferometric visibility $\|g^{(1)}(\tau)\|$ still differ significantly in temporal profiles and/or timescales, similar to cases presented in Figure 2.4(b) and (c). Therefore, the photon bunching of laser light scattered off a rotating ground glass plate cannot be entirely attributed to phase modulation of the light source.

Summary

In this Chapter, we demonstrated how interferometric photon correlations $g^{(2X)}(\tau)$ can be used to directly compare the second-order photon correlation $g^{(2)}(\tau)$ and interferometric visibility $\|g^{(1)}(\tau)\|$ of a light source. This comparison provides insights to the mechanism which results in the observation of photon bunching. From the interferometric photon correlations $g^{(2X)}(\tau)$, a unimodal distribution around zero-time difference $\tau \approx 0$ suggests that the photon bunching may be related to the phase fluctuation of the light source. Otherwise, a multimodal distribution around zero-time difference $\tau \approx 0$, suggests that the photon bunching is not entirely caused by phase fluctuations in the light source, resulting in a different timescale and/or temporal profile of the second-order photon correlation $g^{(2)}(\tau)$ and interferometric visibility $\|g^{(1)}(\tau)\|$.

Our measurements suggests that the mercury discharge lamp emits thermal light, where its second-order photon correlation $g^{(2)}(\tau)$ and interferometric visibility $\|g^{(1)}(\tau)\|$ not only decay on the same timescale with the same temporal profile, but also obey the Siegert relation. In contrast, we observed that the photon bunching of laser light scattered off a rotating ground glass plate is not from phase fluctuations of the light source, which clearly does not obey the Siegert relation and hence should not be considered as thermal light. This calls into question the suitability of laser light scattered off a rotating ground glass plate as a substitute for a blackbody radiator, which prompts for further investigation.

Chapter 5

Ultrabright bunched light

Bunched light can have useful applications in areas such as imaging [35–37] clock synchronisation [40, 41] and ranging [4, 38, 39]. In these applications, two properties of bunched light are leveraged on: its random phasing, which naturally provides distinct signals even among identically built sources, and photon bunching property, from which timing information can be extracted.

However, in these applications, the usefulness of the bunched light sources is limited by two parameters. First, the brightness of the source must withstand the attenuation by the propagation media and the target of interest. Second, the characteristic timescale of the photon bunching must be sufficiently large to be resolved by state-of-the-art photodetectors. For a bunched light source where its photon bunching originates from phase fluctuations, these two parameters can be jointly characterised by the spectral density of a light source.

Laser are well-known for their high spectral densities. Furthermore, the phase fluctuations in a laser are attributed to quantum uncertainties in its emitters and radiation produced [73], and is referred to as quantum noise. However, in principle, lasers do not exhibit photon bunching from phase fluctuations [6]. This motivates for techniques to construct a bunched light source from a laser, utilising its high spectral density and phase fluctuations from quantum noise.

In this Chapter, we present our technique to generate an ultrabright source of bunched light using the phase fluctuations originating from quantum noise in a laser. To do this, we superpose laser light with itself beyond its coherence time using an asymmetric Mach-Zehnder interferometer, which produces an output light field randomly phased by the quantum noise of the laser. To our knowledge, this

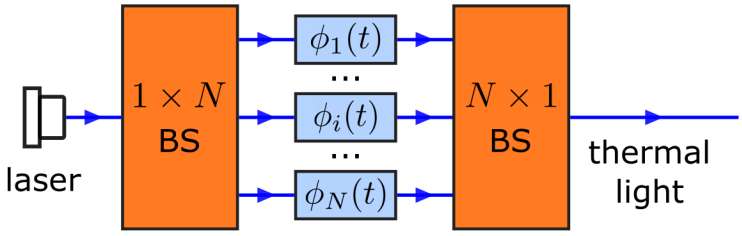

Figure 5.1: Schematic of a general approach to produce thermal light from coherent light. Coherent light from a laser is sent to a $1 \times N$ beam splitter represented by box labelled $1 \times N$ BS. which splits the light into N different modes. A different time-varying random phase modulation $\phi_i(t)$ is applied to each mode. The N modes are then recombined or projected into a single mode represented as a N to 1 beam combiner ($N \times 1$ BS). The light output from this beam combiner approaches thermal light.

is the first demonstrationn of using this technique as a bunched light source. This technique has previously been used to generate random intensity spikes as part of a quantum random number generator [51, 52].

5.1 Superposition of uncorrelated fields

Towards generating a bunched light source, we study the model of thermal light, an example of bunched light where its photon bunching originates from phase fluctuations. We recall that thermal light can be modelled as a large ensemble of emitters, emitting independently phased coherent light fields in Equation 4.1:

$$E(t) = \sum_{j=1}^{N} \frac{1}{\sqrt{N}} E_j(t).$$

From Equation 4.1, an approach to produce thermal light from coherent light may be to use an N-path interferometer as shown in Figure 5.1. The coherent light is divided into N spatial modes using a 1 to N beam splitter. The temporal correlation between spatial modes is removed by applying a different random time-varying phase modulation $\phi_i(t)$ to each spatial mode. The N spatial modes are then recombined into a single spatial mode again.

Alternatively, the same effect can be achieved by superposing multiple coherent light sources that are phase independent with each other. This technique has been

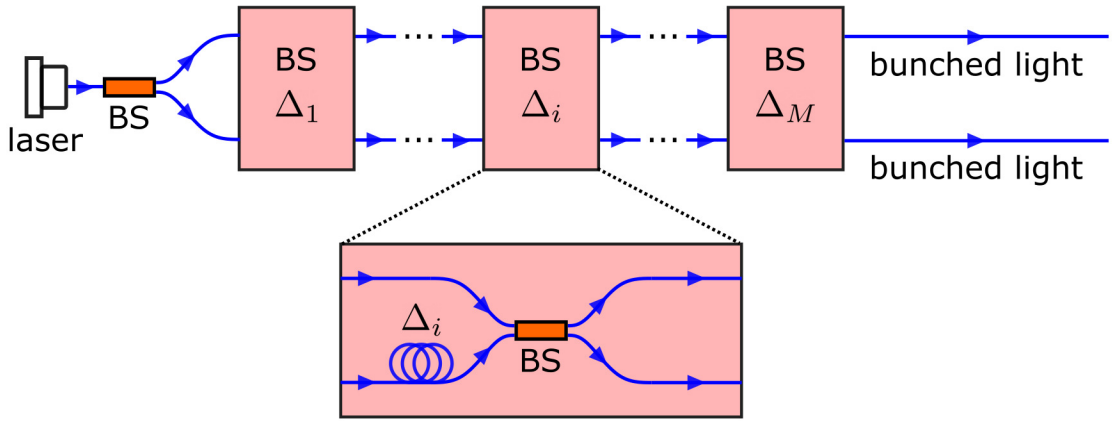

Figure 5.2: Proposed setup for converting coherent light to bunched light. A single spatial mode of coherent light from a laser is split into two spatial modes via a beamsplitter (BS). A delay Δ_1 significantly longer than the coherence time of coherent light is added to one of the modes. The two spatial modes recombine again at another beam splitter, and splits into two modes. In one of the modes, a delay Δ_2 using the conditions in Equation 5.1 is added to one of the modes, the two modes are recombined and splitter at another beamsplitter. The process of adding a delay Δ_i to one arm, recombining and splitting is iterated M times (see inset for the setup in each iteration). At the last beam splitter, either one of the two output modes can be used as a light source approaching thermal light.

proposed by Glauber in the footnote of Reference [69].

The challenge in these approaches is to efficiently recombine N independent spatial modes into a single spatial mode. Ideally, this requires an N-to-1 beam combiner with minimal losses as shown in Figure 5.1. However, at the point of writing this thesis, such a device does not exist. A closely related device is the photonic lantern [74], which combines multiple single mode optical fibres into a multimode optical fibre.

To minimise the losses in superposing these N spatial modes, we present an alternative approach which uses a cascade of 2-to-2 beam splitters to generate the multi-path interferometer shown in Figure 5.2. The coherent light is divided equally into two spatial modes by a $50:50$ beamsplitter as it enters the setup. To ensure that these two modes have uncorrelated phases when they recombine at the next beamsplitter, the temporal correlation between the two modes is removed by introducing a propagation delay Δ_1 to one of the modes, with Δ_1 much longer than

the coherence time τ_c of the light. The next 50 : 50 beamsplitter recombines these two modes, and outputs them again into two spatial modes. The process repeats with introducing a propagation delay Δ_i in one of the modes, recombining the two modes, and then splitting again into two modes is repeated M times.

This cascade of M modules that takes in two spatial modes, adding a delay to one mode, putting them in a superposition and splitting them into two spatial modes results in an interferometer with 2^M possible paths which the initial coherent light field may propagate through. For the coherent light field from each of these paths to be independently phased from one another, the propagation delays Δ_i introduced have to satisfy

$$\left\| \Delta_i - \sum^{j \neq i} \Delta_j \right\| \gg \tau_c \,, \tag{5.1}$$

with a simple way to do so by using the relationship

$$\begin{aligned} \Delta_{i+1} &= 2\Delta_i \,, \\ \Delta_1 &\gg \tau_c \,. \end{aligned} \tag{5.2}$$

At the output of this interferometer, the resultant light field is a superposition of 2^M independently phased coherent light fields, which approaches the thermal light model in Equation 4.1 for a large M. As the phase fluctuation of each coherent light field in principle originates from the quantum noise of the laser, the random phasing after superposing these fields is also a result of quantum noise.

Using Equation 2.11, this output light field has a second-order photon correlation

$$g^{(2)}(\tau) = 1 + \left(1 - \frac{1}{2^M}\right) \left\| g^{(1)}(\tau) \right\|^2 , \tag{5.3}$$

where $\|g^{(1)}(\tau)\|$ is the interferometric visibility of the laser source.

Assuming the interferometric visibility $\|g^{(1)}(0)\| = 1$, the relationship between photon bunching amplitude $g^{(2)}(0) - 1$ of this output light field and the number of modules M used is shown in Figure 5.3. Even for $M = 3$, one expects a photon bunching amplitude $g^{(2)}(0) - 1 = 0.875$, which is already 93.75% of the photon bunching amplitude $g^{(2)}(0) - 1 = 1$ of ideal thermal light. We note that for $M = 0$, Equation 5.3 predicts a second-order photon correlation $g^{(2)}(\tau) = 1$, which agrees with the expectation for a single coherent mode.

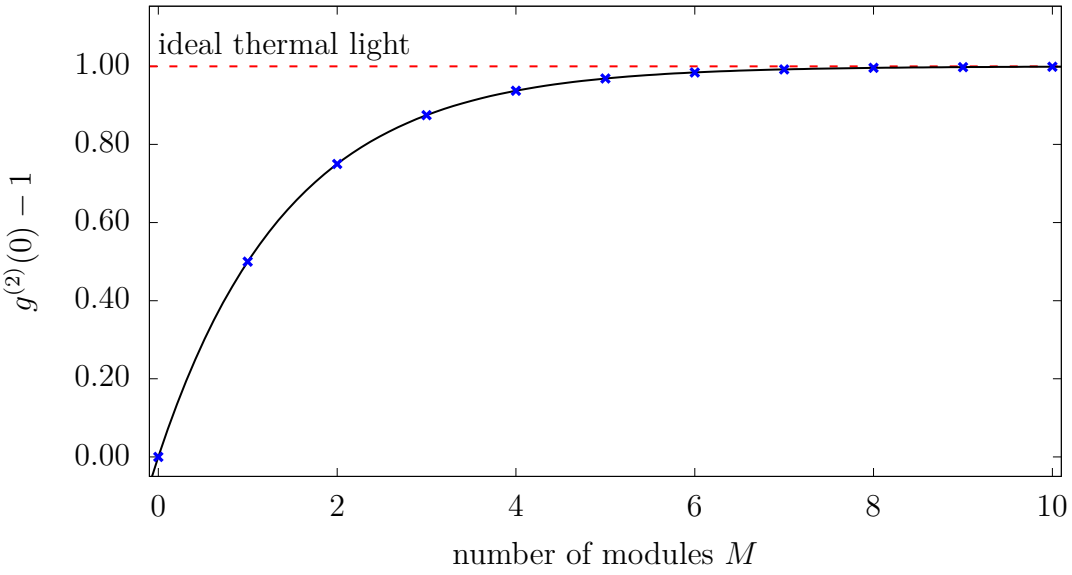

Figure 5.3: Expected photon bunching amplitude $g^{(2)}(0) - 1$ for different number of modules M described in Figure 5.2. The black solid curve shows relation between photon bunching amplitude $g^{(2)}(0) - 1$ and using Equation 5.3, and the blue crosses mark out values for integer M. The red dotted line shows photon bunching amplitude $g^{(2)}(0) - 1 = 2$ for an ideal thermal light.

5.2 Superposition of two coherent modes

We demonstrate our technique towards converting coherent light from the laser to bunched light using the setup shown in Figure 5.4. This is a variation of the setup in Figure 5.2 when $M = 1$. This converts the single coherent mode into a superposition of two independent modes.

A laser operating above the lasing threshold emits light with a central wavelength about 780 nm. Using the techniques in Chapter 3, we measure a coherence time of $\tau_c = 194 \pm 1$ ns and a proportion of coherent light emitted by the laser to be about $\rho = 0.940$, within a 90% confidence interval of 0.931 to 0.948.

To create an asymmetric Mach-Zehnder interferometer to superpose two uncorrelated modes of coherent light, the light is first sent through a single-mode fused fibre coupler which acts as a beam splitter and distributes the light into two spatial modes. The two outputs of the fused fibre coupler terminate with aspheric lenses preparing collimated beams in free space. In each beam path, a half-wave plate and quarter-wave plate for 780 nm was introduced, and adjusted to match

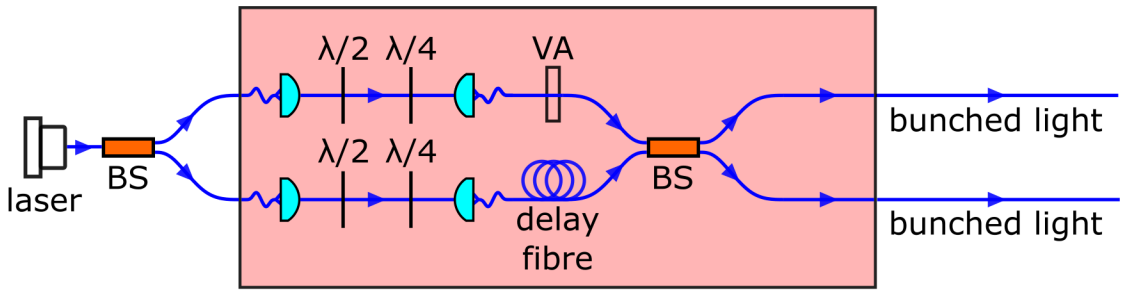

Figure 5.4: Setup for converting coherent light to bunched light. A single spatial mode of coherent light from a laser is split into two spatial modes via a beamsplitter (BS). In both arms of the interferometer a half-wave plate ($\lambda/2$) and quarter wave-plate ($\lambda/4$) can be adjusted to match the polarisations of the two modes when they meet at a second beam splitter. A propagation delay Δ_{bun} significantly longer than the coherence time of the coherent light is introduced to one of the modes via an optical fiber. In the other mode, we attenuate the optical power transmitted through this arm by adjusting the fibre optic coupling, modelled here as a variable attenuator (VA). This is to vary the power fraction α between the two modes when they recombine again at another beam splitter, producing a superposition of two independently phased coherent light fields. The two output mode superposes with each other when they meet at a second beam splitter. One of the two output modes from the interferometer is used as a bunched light source.

the polarisation of the two light fields when they combine at a second fused fibre coupler later. Using another pair of aspheric lenses, we coupled light from one of the beams into a series of optical fibres with a combined length of about 280 m, which introduced a propagation delay $\Delta_{\text{bun}} \approx 1.4\,\mu$s. The other end of this fibre is connected to one of the input ports of a second fused fibre coupler using fibre mating connectors. The other input of this fused fibre coupler receives the beam without delay. To match the different losses of the two paths, we realised an attenuation to the beam without delay by misalignment of the beam entering the the input port of the second fused fibre coupler.

The second fused fibre coupler, closes the asymmetric interferometer, and light emerging from one of the output ports is used as the light source for a superposition of two coherent modes with independent phases. We matched the polarisations of these two superposed modes by introducing an in-line fibre optic polariser after the output of the interferometer. The optical power was measured after the polariser, and

the half-wave and quarter-wave plates were adjusted to maximise the transmission of light from each mode through the polariser. The polariser is subsequently removed after the polarisations are matched.

Ideally, the conversion of laser light to bunched light expects an attenuation of 3 dB, which is due to dividing the optical power equally between the two output modes of the interferometer. We measured about 30 mW of optical power entering the asymmetric Mach-Zehnder interferometer, and 1 mW exiting from one port of the interferometer. The optical losses is mainly attributed to the splicing losses in the optical fibre which introduced the propagation delay Δ_{bun}. This also required a similar attenuation in the non-delayed path of the interferometer to match the losses. An optical power of 1 mW from one port of the interferometer translates to about 4×10^{16} photons per second, at a wavelength of 780 nm.

The superposition of the light field at a output of the interferometer is

$$E_{\text{bun}}(t) = \sqrt{\alpha}E(t) + \sqrt{(1-\alpha)}E(t+\Delta_{\text{bun}})\,, \tag{5.4}$$

where the unindexed fields $E(t)$ represents the light field from the laser, and α represents the power fraction of the non-delayed field at one of the output port of the interferometer. In the above model, the magnitude of the electric fields were normalised such that $\|E_{\text{bun}}(t)\| = \|E(t)\| = \|E(t+\Delta_{\text{bun}})\|$.

To measure the second-order photon correlation $g^{(2)}(\tau)$ of the output light field from the interferometer, we constructed a Hanbury-Brown and Twiss type interferometer by obstructing one arm of the asymmetric Mach-Zehnder interferometer to extract interferometric photon correlations $g^{(2X)}(\tau)$, as shown in Figure 2.2(b). Light from the bunched light source is output into two spatial modes. The light from each spatial mode is sent into actively quenched silicon avalanche photodetectors with a timing resolution of about 40 ps. The detection timings of these photevents are logged with a timestamp card with 2 ns resolution. From the timestamps, photon correlations are extracted using the methods described in Chapter 2. The measured the second-order photon correlation $g^{(2)}(\tau)$ for the bunched light for different power α is shown in Figure 5.5(a).

Using the superposition field in Equation 5.4, and the correlations in Equa-

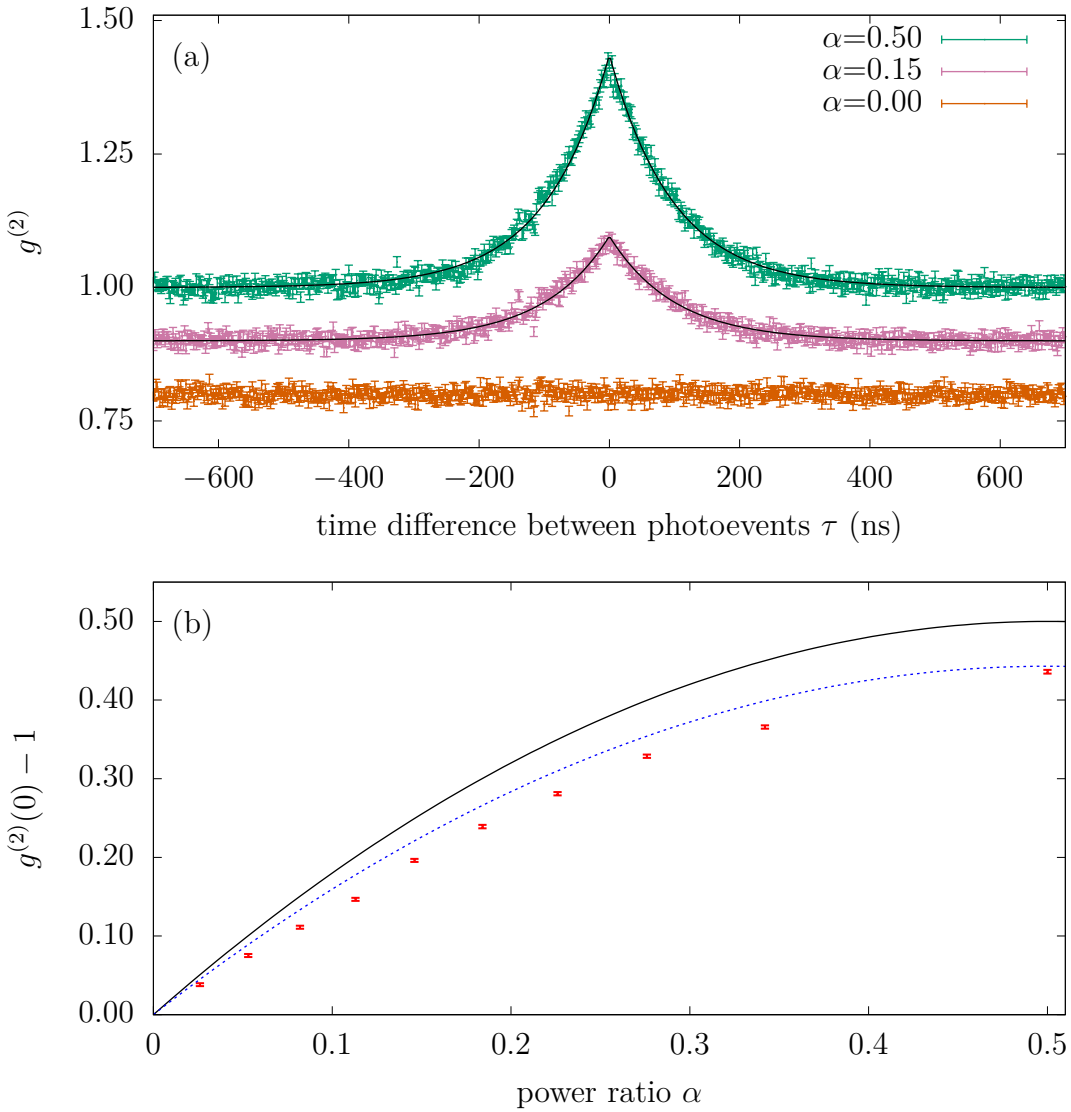

Figure 5.5: (a) Second-order photon correlations $g^{(2)}(\tau)$ extracted from the superposition of two independent coherent modes at power fraction $\alpha = 0.50$ (green), 0.15 (pink) and 0 (orange). The pink and green curves are vertically offset by -0.1 and -0.2 respectively for visual clarity of data. The solid black curves shows the fit of the curves of $g^{(2)}(\tau)$ $\alpha = 0.50$ and 0.15 to Equations 5.6 and 5.5. (b) Photon bunching amplitude $g^{(2)}(0) - 1$ for different power fractions α between the non-delayed light field $E(t)$ and the total power after combining with the delayed light field $E_{\text{bun}}(t)$. The red points show the measured photon bunching amplitude $g^{(2)}(0) - 1$ extracted from the fit of second-order photon correlations $g^{(2)}(\tau)$ to Equations 5.5 and 5.6 for different α. The black solid curve shows the relationship between photon bunching amplitude $g^{(2)}(0) - 1$ and power fraction α between the two modes using Equation 5.5, for a laser that fully emits coherent light, i.e. a fraction of coherent light $\rho = 1$. The blue dashed curve shows the same relationship accounting for the fraction of coherent light emitted by the laser $\rho = 0.940$ using Equation 5.6.

tions 4.5-4.7, the second-order photon correlation of E_{bun} is

$$\begin{aligned} g^{(2)}(\tau) &= \alpha^2 + (1-\alpha)^2 + 2\alpha(1-\alpha) + 2r(1-\alpha)\left\|\langle E^*(t)E(t+\tau)\rangle\right\|^2 \\ &= 1 + 2\alpha\,(1-\alpha)\left\|g^{(1)}(\tau)\right\|^2. \end{aligned} \tag{5.5}$$

where $E(t)$ is the electric field of the laser source.

To fit the second-order photon correlation $g^{(2)}(\tau)$ of bunched light to Equation 5.5, we require a suitable model for the interferometric visibility $\|g^{(1)}(\tau)\|$. We assume the laser emits a mixture of coherent light and broadband thermal light, which has an interferometric visibility in the form of Equation 3.2:

$$\begin{aligned} \left\|g^{(1)}_{\text{mix}}(\tau)\right\|^2 = \rho^2 &\left\|g^{(1)}_{\text{coh}}(\tau)\right\|^2 + (1-\rho)^2\left\|g^{(1)}_{\text{unc}}(\tau)\right\|^2 \\ &+ 2\rho(1-\rho)\,\Re[g^{(1)}_{\text{coh}}(\tau)\,g^{(1)*}_{\text{unc}}(\tau)] \\ &+ 2\rho(1-\rho)\,\Re[g^{(1)}_{\text{coh}}(\Delta)\,g^{(1)*}_{\text{unc}}(\Delta)]\,. \end{aligned}$$

We assumed that the light field uncorrelated to the coherent light to be broadband, such that its coherence time τ_c is much shorter than the timing response of the photodetectors. The convolution of this characteristic timescale with the detector timing response leads to the measured interfometric visibility $\|g^{(1)}_{\text{unc}}(\tau)\| \approx 0$ for the light field uncorrelated to the coherent light in the mixture. We further assume a Lorentzian spectral lineshape for the coherent light component in the mixture, and the interferometric visibility for the light emitted by the laser is

$$\left\|g^{(1)}(\tau)\right\|^2 \approx \rho^2 \exp\left(-\left\|\frac{2\tau}{\tau_c}\right\|\right), \tag{5.6}$$

where ρ is the fraction of coherent light emitted by the laser. Using Equation 5.5 and 5.6, and the fraction $\rho = 0.94$ of coherent light emitted by the input laser, we predict a photon bunching amplitude $g^{(2)}(0) - 1 = 0.44$ for our bunched light source at a power ratio $\alpha = 0.5$.

5.3 Photon bunching related to phase fluctuations

To understand if the photon bunching in the bunched light source is related to its phase fluctuations, we use interferometric photon correlations $g^{(2X)}(\tau)$ to compare the interferometric visibility-square $\|g^{(1)}_{\text{bun}}(\tau)\|^2$ of the bunched light source with its second-order photon correlation $g^{(2)}(\tau)$.

From Equation 5.4 the interferometric visibility of the bunched light is

$$\begin{aligned}\left\|g^{(1)}_{\text{bun}}(\tau)\right\| &= \left\|\frac{\langle E^*_{\text{bun}}(t)E_{\text{bun}}(t+\tau)\rangle}{\langle E^*_{\text{bun}}(t)E_{\text{bun}}(t)\rangle}\right\| \\ &= \left\|g^{(1)}(\tau)\right\| + \sqrt{\alpha(1-\alpha)}\left[\left\|g^{(1)}(\tau-\Delta_{\text{bun}})\right\| + \left\|g^{(1)}(\tau+\Delta_{\text{bun}})\right\|\right],\end{aligned} \tag{5.7}$$

where the unindexed interferometric visibility $\|g^{(1)}(\tau)\|$ terms are for the electric field of the laser $E(t)$. We note here that the terms containing Δ_{bun} are due to correlations of the light field with its own delayed field. To remove those terms, the technique to generate the bunched light can be modified by replacing the delay fibre with a phase modulator with a randomised input.

For a delay significantly longer than the coherence time of the light $\Delta \gg \tau_c$, the interferometric visibility-square is

$$\left\|g^{(1)}_{\text{bun}}(\tau)\right\|^2 = \left\|g^{(1)}(\tau)\right\|^2 + \alpha(1-\alpha)\left[\left\|g^{(1)}(\tau-\Delta_{\text{bun}})\right\|^2 + \left\|g^{(1)}(\tau+\Delta_{\text{bun}})\right\|^2\right]. \tag{5.8}$$

Using Equation 5.5 and 5.8, the interferometric photon correlation (Equation 2.9) for the bunched light source is

$$\begin{aligned}g^{(2X)}_{\text{bun}}(\tau) = 1 &+ \frac{2\alpha\,(1-\alpha)-1}{2}\left\|g^{(1)}(\tau)\right\|^2 \\ &+ \frac{\alpha\,(1-\alpha)}{2}\left[\left\|g^{(1)}(\tau-\Delta_{\text{int}})\right\|^2 + \left\|g^{(1)}(\tau+\Delta_{\text{int}})\right\|^2\right] \\ &- \frac{\alpha\,(1-\alpha)}{2}\left[\left\|g^{(1)}(\tau-\Delta_{\text{bun}})\right\|^2 + \left\|g^{(1)}(\tau+\Delta_{\text{bun}})\right\|^2\right],\end{aligned} \tag{5.9}$$

where Δ_{int} is the propagation delay in the asymmetric Mach-Zehnder interferometer used to extract interferometric photon correlations $g^{(2X)}(\tau)$, while the propagation delay Δ_{bun} is introduced in the asymmetric Mach-Zehnder interferometer to generate the bunched light. Here, the interferometric visibility $\|g^{(1)}(\tau)\|$ terms are for the electric field of the laser.

We extract the interferometric photon correlations $g^{(2X)}(\tau)$ by sending light through an asymmetric Mach-Zehnder interferometer with a propagation delay $\Delta_{\text{int}} \approx 2\,\mu$s using an optical fibre about 400 m in length. We used the same photodectors and timestamps as those used in extracting its second-order photon correlation $g^{(2)}(\tau)$ in Page 51.

The interferometric photon correlations $g^{(2X)}(\tau)$ for power fractions $\alpha = 0$ and 0.5 are shown in Figure 5.6. From the interferometric photon correlations $g^{(2X)}(\tau)$,

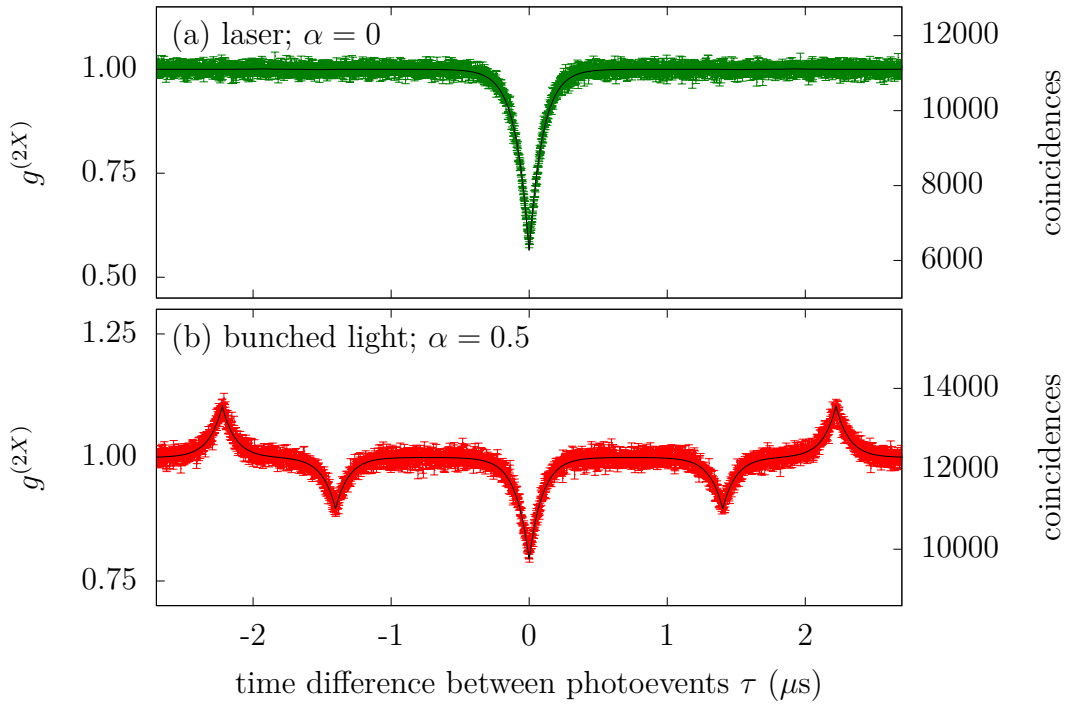

Figure 5.6: Interferometric photon correlations $g^{(2)}(\tau)$ for (a) laser light, for a power fraction $\alpha = 0$, (b) bunched light source, for a power fraction $\alpha = 0.5$. The solid black lines are fitted curves to Equation 5.9. From the fit, we extracted the characteristic timescale of interferometric visibility $\|g^{(1)}(\tau)\|$ to be (a)$\tau_c = 194 \pm 1$ ns and (b) $\tau_c = 193 \pm 2$ ns. The additional dips are centered around $\tau \approx 1.4\,\mu$s are attributed to correlations of the field with itself after delay Δ_{bun} in Equation 5.8.

the distribution around zero-time difference $\tau \approx 0$ appears to be unimodal, showing only a dip centered around $\tau = 0$. This suggests that the photon bunching observed is related to the phase fluctuations in the bunched light source. The fit of the interferometric photon correlations $g^{(2X)}(\tau)$ to Equation 5.9 had a reduced-$\chi^2 = 1.09$, suggesting a good agreement with the model.

From the fit, we extracted a characteristic timescale $\tau_c = 193 \pm 2$ ns of the interferometric visibility $\|g^{(1)}(\tau)\|$. Using Equation 3.16, this translates to a 1.6 MHz bandwidth or 3.4 fm linewidth for a central wavelength 780 nm. We divide the optical power of our bunched light of 4×10^{16} photons per second by its spectral linewidth to obtain its spectral brightness of this light source of about 1×10^{22} photons per second per nm bandwidth.

Although the unimodal distribution suggests the photon bunching signature

$g^{(2)}(\tau) - 1$ and interferometric visibility-square $\|g^{(1)}(\tau)\|^2$ have the same timescale and profile, they do not cancel out completely here due to difference in amplitudes. This means that the second-order photon correlation $g^{(2)}(\tau)$ and interferometric visibility-square $\|g^{(1)}(\tau)\|^2$ does not strictly follow the Siegert relation, unlike thermal light. This is due to using only two independent emitters, whereas a "true" thermal light source would have a large number of emitters. With an increased number of cascaded Mach-Zehnder interferometers to create more paths as described in Figure 5.2, we would expect the Siegert relation to be followed. Nevertheless, the interferometric photon correlations $g^{(2X)}(\tau)$ suggests that we have prepared a bunched light source with the photon bunching from the phase fluctuations of the laser.

In our experiment, we measured an attenuatation of 14.5 dB, mainly attributed to losses from fibre optic splicing, mating, and coupling.

Summary

We presented a general approach towards generating bunched light from a coherent light source. A coherent light field can be split into N different modes, with each mode independently and randomly phase modulated, before combining in a single mode again. Our approach towards this is to cascade a series of M asymmetric Mach-Zehnder interferometers, which forms a multi-path interferometer with 2^M paths.

We demonstrated a bunched light source by sending laser light through a single asymmetric Mach-Zehnder interferometer. This superposes the laser light field with itself outside of its coherence time. The resulting output field can be modelled as a superposition of two independent coherent fields which produces a theoretical photon bunching amplitude $g^{(2)}(0) - 1 = 0.5$. Experimentally, we observed a photon bunching amplitude $g^{(2)}(0) - 1 = 0.437 \pm 0.002$.

From interferometric photon correlations $g^{(2X)}(\tau)$, the coherence time τ_c of the bunched light source is about 190 ns, translating to a linewidth approximately 3.4 fm. At a power of 1 mW, this linewidth leads to spectral density of 10^{22} photons per second per nm bandwidth, 10000 times higher in spectral density than the bunched light source with the highest spectral density known to us in literature [4].

The interferometric photon correlation $g^{(2X)}(\tau)$ of the bunched light also suggests that the photon bunching is related to the random phase fluctuations of the bunched light source, which is attributed to quantum noise of the laser.

Chapter 6

Summary and Outlook

The main result of this thesis was the presentation of an ultrabright narrowband source of bunched light with a second-order photon correlation $g^{(2)}(0) = 1.437 \pm 0.002$, close to the theoretical value of $g^{(2)}(0) = 1.50$ for this configuration. Using interferometric photon correlations $g^{(2X)}(\tau)$, a direct comparison between the interferometric visibility $\|g^{(1)}(\tau)\|$ and the second-order photon correlation $g^{(2)}(\tau)$ of the bunched was made, and it suggests that the photon bunching of the bunched light source is related to phase fluctuations.

We measured an output power of 1 mW for the bunched light, which allows for attenuation up to 140 dB by the propagation media before the signal is comparable to noise in the single photon detectors. We also measured and a coherence time of ~ 190 ns for our bunched light source. This translates to a spectral brightness of about 10^{22} photoevents per second per nanometer linewidth. This is 10^4 times brighter than the brightest bunched light source known to us, which is based on a laser operating below its lasing threshold [4]. The brightness can be easily increased with a higher power laser input, and is only limited by the damage threshold of the optics.

The characterisation techniques we developed from interferometric photon correlations $g^{(2X)}(\tau)$ was also applied to other sources. One technique was the ability to extract the coherence time and fraction of coherent light as demonstrated in Chapter 3 and 5.

Another technique was to directly compare the interferometric visibility $\|g^{(1)}(\tau)\|$ and the second-order photon correlation $g^{(2)}(\tau)$ in a single measurement. From this, we determine if photon bunching can be attributed to the light source's phase fluctuations. Using this technique, we showed that the emission from a mercury

discharge lamp is indeed a source of thermal light. On the other hand, we show that the photon bunching of laser light scattered off a rotating ground glass plate does not purely originate from phase fluctuations.

Towards applications resilient to high losses

The bunched light source presented in this thesis have addressed the initial motivation of a brighter narrowband bunched light source, remarkably without requiring an external source of modulation. Future works may include demonstrations of this light source in applications such optical ranging [4] and clock synchronisation [40, 41], in more adverse conditions such as greater losses from distance, propagation media or less cooperative targets.

During the preparation of this thesis, we discovered that the method of sending laser light through an asymmetric Mach-Zehnder interferometer has also been used to generate random intensity spikes for applications in high bit rate quantum random number generators [51, 52]. This further substantiates the potential of using the quantum noise from a laser as a resource for randomness.

Interacting bunched light with quantum systems

Although there is a fundamental interest in studying interactions between atoms and light of different statistics [75, 76], the popular focus of atom-light interaction experiments tends to be on using coherent light sources and single photon sources [77–79]. This may be substantiated by our failure to find reported experiments of atom-light interactions with incoherent light sources during our literature search. Apart from these interactions, other effects, such as stochastic resonance [80–82] in atomic systems using incoherent light as a noise source, would also be of fundamental interest to investigate.

Furthermore, there has been proposed techniques of using quantum repeaters and memories to enhance the imaging capabilities of astronomical telescopes [83–87]. Towards this application, preliminary studies of interaction between quantum systems and incoherent light, which may be similar in nature to light from celestial objects, has to be conducted.

A probable challenge in performing these experiments with incoherent light may

be due to the low spectral density of existing incoherent light sources, which results in a low probability of interaction, rendering experiments impractically time-consuming. With our technique for a bright source of narrowband bunched light, along with the other approaches highlighted in Chapter 5, these experiments may come closer to realisation.

Further applications of interferometric photon correlations

This technique may be further applied to areas such as in laser physics, where one may be interested in measuring the fraction of spontaneous emission that is emitted into the laser mode [88, 89], or in continuous-variable quantum key distribution, where one may be interested in characterising the amount of optical noise in the channel or source, such as in [90].

This can complement the widely used second-order photon correlations $g^{(2)}(\tau)$ traditionally used to distinguish between light sources of different nature, such as coherent and incoherent light. Challenges in clearly distinguishing between coherent and incoherent light arise in situations such as, using detectors with limited timing resolution [49], or unintended amplitude modulation of the light source [2]. Examples of unintended amplitude modulation include: scattering from interstellar dust in observations of celestial light, such as astrophysical lasers [91–94] and from technosignatures [95–97] or in random lasers [98–100], which relies on the scattering of particles for optical feedback.

Even for well-established techniques, such as dynamic light scattering [14], which uses the second-order photon correlation $g^{(2)}(\tau)$ of laser light scattered from particles to study the dynamics of particles, being able to also simultaneously extract the interferometric visibility $\left\|g^{(1)}(\tau)\right\|$ from interferometric photon correlations $g^{(2X)}(\tau)$ may pave the way for more in-depth analysis. The required modifications from a setup extracting second-order photon correlations $g^{(2)}(\tau)$ to a setup extracting interferometric photon correlations $g^{(2X)}(\tau)$ would not be complex; the main difference is an additional interferometer.

Bibliography

[1]A. Lebreton, I. Abram, R. Braive, I. Sagnes, I. Robert-Philip, and A. Beveratos, "Theory of interferometric photon-correlation measurements: differentiating coherent from chaotic light", Phys. Rev. A **88**, 013801 (2013).

[2]A. Lebreton, I. Abram, R. Braive, I. Sagnes, I. Robert-Philip, and A. Beveratos, "Unequivocal differentiation of coherent and chaotic light through interferometric photon correlation measurements", Phys. Rev. Lett. **110**, 163603 (2013).

[3]X. J. Yeo, E. Ernst, A. Leow, J. Hwang, L. Shen, C. Kurtsiefer, and P. K. Tan, "Direct measurement of the coherent light proportion from a practical laser source", Phys. Rev. A **109**, 013706 (2024).

[4]P. K. Tan, X. J. Yeo, A. Z. W. Leow, L. Shen, and C. Kurtsiefer, "Practical range sensing with thermal light", Phys. Rev. Appl. **20**, 014060 (2023).

[5]R. Loudon, "The quantum theory of light", (Oxford, UK, 2000).

[6]M. Fox, "Quantum optics: an introduction", Oxford Master Series in Physics (OUP Oxford, 2006).

[7]P. K. Tan, G. H. Yeo, H. S. Poh, A. H. Chan, and C. Kurtsiefer, "Measuring temporal photon bunching in blackbody radiation", The Astrophysical Journal Letters **789**, L10 (2014).

[8]W. Guerin, A. Dussaux, M. Fouché, G. Labeyrie, J.-P. Rivet, D. Vernet, F. Vakili, and R. Kaiser, "Temporal intensity interferometry: photon bunching in three bright stars", Monthly Notices of the Royal Astronomical Society **472**, 4126–4132 (2017).

[9]Y.-H. Deng, H. Wang, X. Ding, Z.-C. Duan, J. Qin, M.-C. Chen, Y. He, Y.-M. He, J.-P. Li, Y.-H. Li, L.-C. Peng, E. S. Matekole, T. Byrnes, C. Schneider, M. Kamp, D.-W. Wang, J. P. Dowling, S. Höfling, C.-Y. Lu, M. O. Scully, and J.-W. Pan,

"Quantum interference between light sources separated by 150 million kilometers", Phys. Rev. Lett. **123**, 080401 (2019).

[10]R. H. Brown and R. Q. Twiss, "Correlation between photons in two coherent beams of light", Nature **177**, 27–29 (1956).

[11]G. A. Rebka and R. V. Pound, "Time-correlated photons", Nature **180**, 1035–1036 (1957).

[12]B. L. Morgan and L. Mandel, "Measurement of photon bunching in a thermal light beam", Phys. Rev. Lett. **16**, 1012–1015 (1966).

[13]P. K. Tan, A. H. Chan, and C. Kurtsiefer, "Optical intensity interferometry through atmospheric turbulence", Monthly Notices of the Royal Astronomical Society **457**, 4291–4295 (2016).

[14]R. Pecora, "Doppler Shifts in Light Scattering from Pure Liquids and Polymer Solutions", The Journal of Chemical Physics **40**, 1604–1614 (1964).

[15]F. T. Arecchi, M. Giglio, and U. Tartari, "Scattering of coherent light by a statistical medium", Phys. Rev. **163**, 186–194 (1967).

[16]D. Dravins, T. Lagadec, and P. D. Nuñez, "Optical aperture synthesis with electronically connected telescopes", Nature Communications **6**, 6852 (2015).

[17]P. Lassègues, M. A. F. Biscassi, M. Morisse, A. Cidrim, N. Matthews, G. Labeyrie, J. Rivet, F. Vakili, R. Kaiser, W. Guerin, et al., "Field and intensity correlations: the siegert relation from stars to quantum emitters", Eur. Phys. J. D **76**, 246 (2022).

[18]W. Martienssen and E. Spiller, "Coherence and Fluctuations in Light Beams", Am. J. Phys. **32**, 919–926 (1964).

[19]T. Asakura, "Spatial coherence of laser light passed through rotating ground glass", Opto-electronics **2**, 115–123 (1970).

[20]P. N. Pusey, "Photon correlation study of laser speckle produced by a moving rough surface", J. Phys. D **9**, 1399–1409 (1976).

[21]P. Hong, J. Liu, and G. Zhang, "Two-photon superbunching of thermal light via multiple two-photon path interference", Phys. Rev. A **86**, 013807 (2012).

[22]T. A. Kuusela, "Measurement of the second-order coherence of pseudothermal light", Am. J. Phys. **85**, 289–294 (2017).

[23]D. Ferreira, R. Bachelard, W. Guerin, R. Kaiser, and M. Fouché, "Connecting field and intensity correlations: the siegert relation and how to test it", Am. J. Phys. **88**, 831–837 (2020).

[24]X. Tang, Y. Zhang, X. Guo, L. Cui, X. Li, and O. Z. Y., "Phase dependent hanbury-brown and twiss effect", 2023.

[25]C.-H. Lee, Y. Kim, D.-G. Im, U.-S. Kim, V. Tamma, and Y.-H. Kim, "Coherent two-photon lidar with incoherent light", Phys. Rev. Lett. **131**, 223602 (2023).

[26]A. T. M. A. Rahman and P. F. Barker, "Optical levitation using broadband light", Optica **7**, 906–912 (2020).

[27]M. Aßmann, F. Veit, M. Bayer, C. Gies, F. Jahnke, S. Reitzenstein, S. Höfling, L. Worschech, and A. Forchel, "Ultrafast tracking of second-order photon correlations in the emission of quantum-dot microresonator lasers", Phys. Rev. B **81**, 165314 (2010).

[28]P. Janassek, A. Herdt, S. Blumenstein, and W. Elsä, "Ghost spectroscopy with classical correlated amplified spontaneous emission photons emitted by an erbium-doped fiber amplifier", Applied Sciences **8**, `10.3390/app8101896` (2018).

[29]P. G. Kwiat, K. Mattle, H. Weinfurter, A. Zeilinger, A. V. Sergienko, and Y. Shih, "New high-intensity source of polarization-entangled photon pairs", Phys. Rev. Lett. **75**, 4337–4341 (1995).

[30]Z. Zhang, S. Mouradian, F. N. C. Wong, and J. H. Shapiro, "Entanglement-enhanced sensing in a lossy and noisy environment", Phys. Rev. Lett. **114**, 110506 (2015).

[31]Y.-C. Jeong, K.-H. Hong, and Y.-H. Kim, "Bright source of polarization-entangled photons using a ppktp pumped by a broadband multi-mode diode laser", Opt. Express **24**, 1165–1174 (2016).

[32]A. Lohrmann, A. Villar, A. Stolk, and A. Ling, "High fidelity field stop collection for polarization-entangled photon pair sources", Applied Physics Letters **113**, 171109 (2018).

[33]T. J. Steiner, J. E. Castro, L. Chang, Q. Dang, W. Xie, J. Norman, J. E. Bowers, and G. Moody, "Ultrabright entangled-photon-pair generation from an AlGaAs-on-insulator microring resonator", PRX Quantum **2**, 010337 (2021).

[34]D. G. England, B. Balaji, and B. J. Sussman, "Quantum-enhanced standoff detection using correlated photon pairs", Phys. Rev. A **99**, 023828 (2019).

[35]A. Valencia, G. Scarcelli, M. D'Angelo, and Y. Shih, "Two-photon imaging with thermal light", Phys. Rev. Lett. **94**, 063601 (2005).

[36]B. I. Erkmen and J. H. Shapiro, "Unified theory of ghost imaging with gaussian-state light", Phys. Rev. A **77**, 043809 (2008).

[37]E. D. Lopaeva, I. Ruo Berchera, I. P. Degiovanni, S. Olivares, G. Brida, and M. Genovese, "Experimental realization of quantum illumination", Phys. Rev. Lett. **110**, 153603 (2013).

[38]J. Zhu, X. Chen, P. Huang, and G. Zeng, "Thermal-light-based ranging using second-order coherence", Appl. Opt. **51**, 4885–4890 (2012).

[39]S. Frick, A. McMillan, and J. Rarity, "Quantum rangefinding", Opt. Express **28**, 37118–37128 (2020).

[40]C. Ho, A. Lamas-Linares, and C. Kurtsiefer, "Clock synchronization by remote detection of correlated photon pairs", New Journal of Physics **11**, 045011 (2009).

[41]J. Lee, L. Shen, A. Cerè, J. Troupe, A. Lamas-Linares, and C. Kurtsiefer, "Symmetrical clock synchronization with time-correlated photon pairs", Applied Physics Letters **114**, 101102 (2019).

[42]A. Einstein, "Strahlung-emission und-absorption nach der quantentheorie", Verh. d. Deutsche Physik. Ges. **18**, 318–328 (1916).

[43]W. H. Louisell, A. Yariv, and A. E. Siegman, "Quantum fluctuations and noise in parametric processes. i." Phys. Rev. **124**, 1646–1654 (1961).

[44]J. P. Gordon, W. H. Louisell, and L. R. Walker, "Quantum fluctuations and noise in parametric processes. ii", Phys. Rev. **129**, 481–485 (1963).

[45]B. Hayes, "Computing science: randomness as a resource", American Scientist **89**, 300–304 (2001).

[46]Y. Zhou, F.-l. Li, B. Bai, H. Chen, J. Liu, Z. Xu, and H. Zheng, "Superbunching pseudothermal light", Phys. Rev. A **95**, 053809 (2017).

[47]Y. Zhou, X. Zhang, Z. Wang, F. Zhang, H. Chen, H. Zheng, J. Liu, F.-l. Li, and Z. Xu, "Superbunching pseudothermal light with intensity modulated laser light and rotating groundglass", Optics Communications **437**, 330–336 (2019).

[48]L. Zhang, Y. Lu, D. Zhou, H. Zhang, L. Li, and G. Zhang, "Superbunching effect of classical light with a digitally designed spatially phase-correlated wave front", Phys. Rev. A **99**, 063827 (2019).

[49]D. B. Scarl, "Measurements of photon correlations in partially coherent light", Phys. Rev. **175**, 1661–1668 (1968).

[50]C. H. Henry and R. F. Kazarinov, "Quantum noise in photonics", Rev. Mod. Phys. **68**, 801–853 (1996).

[51]B. Qi, Y.-M. Chi, H.-K. Lo, and L. Qian, "High-speed quantum random number generation by measuring phase noise of a single-mode laser", Opt. Lett. **35**, 312–314 (2010).

[52]H. Guo, W. Tang, Y. Liu, and W. Wei, "Truly random number generation based on measurement of phase noise of a laser", Phys. Rev. E **81**, 051137 (2010).

[53]Y.-S. Choi, M. T. Rakher, K. Hennessy, S. Strauf, A. Badolato, P. M. Petroff, D. Bouwmeester, and E. L. Hu, "Evolution of the onset of coherence in a family of photonic crystal nanolasers", Appl. Phys. Lett. **91**, 031108 (2007).

[54]S. M. Ulrich, C. Gies, S. Ates, J. Wiersig, S. Reitzenstein, C. Hofmann, A. Löffler, A. Forchel, F. Jahnke, and P. Michler, "Photon statistics of semiconductor microcavity lasers", Phys. Rev. Lett. **98**, 043906 (2007).

[55]C. Gies, J. Wiersig, M. Lorke, and F. Jahnke, "Semiconductor model for quantum-dot-based microcavity lasers", Phys. Rev. A **75**, 013803 (2007).

[56]J. Wiersig, C. Gies, F. Jahnke, M. Aßmann, T. Berstermann, M. Bayer, C. Kistner, S. Reitzenstein, C. Schneider, S. Höfling, A. Forchel, C. Kruse, J. Kalden, and D. Hommel, "Direct observation of correlations between individual photon emission events of a microcavity laser", Nature **460**, 245–249 (2009).

[57]S. Kreinberg, W. W. Chow, J. Wolters, C. Schneider, C. Gies, F. Jahnke, S. Höfling, M. Kamp, and S. Reitzenstein, "Emission from quantum-dot high-ßmicrocavities: transition from spontaneous emission to lasing and the effects of superradiant emitter coupling", Light Sci. Appl. **6** (2017).

[58]P. K. Tan and C. Kurtsiefer, "Temporal intensity interferometry for characterization of very narrow spectral lines", Mon. Not. R. Astron. Soc. **469**, 1617–1621 (2017).

[59]X. Brokmann, M. Bawendi, L. Coolen, and J.-P. Hermier, "Photon-correlation fourier spectroscopy", Opt. Express **14**, 6333–6341 (2006).

[60]J. A. Armstrong, "Theory of interferometric analysis of laser phase noise∗", J. Opt. Soc. Am. **56**, 1024–1031 (1966).

[61]M. Born and E. Wolf, "Principles of optics", (Cambridge, UK, 1959).

[62]E. C. G. Sudarshan, "Equivalence of semiclassical and quantum mechanical descriptions of statistical light beams", Phys. Rev. Lett. **10**, 277–279 (1963).

[63]N. Wiener, "Generalized harmonic analysis", Acta Mathematica **55**, 117–258 (1930).

[64]A. Khintchine, "Korrelationstheorie der stationären stochastischen prozesse", Mathematische Annalen **109**, 604–615 (1934).

[65]A. J. F. Siegert, "On the fluctuations in signals returned by many independently moving scatterers", Radiation Laboratory, Massachusetts Institute of Technology (1943).

[66]A. Siegman, "Lasers", (Mill Valley, CA, 1986).

[67]H. Haken, "Light: laser light dynamics", (North-Holland Physics Publishing, Amsterdam, Netherlands, 1981).

[68]T. A. Kuusela, "Electrical source of pseudothermal light", American Journal of Physics **86**, 475–478 (2018).

[69]R. J. Glauber, "The quantum theory of optical coherence", Phys. Rev. **130**, 2529–2539 (1963).

[70]C. J. Sansonetti and D. Veza, "Doppler-free measurement of the 546 nm line of mercury", Journal of Physics B: Atomic, Molecular and Optical Physics **43**, 205003 (2010).

[71]L. E. Estes, M. Narducci, and R. A. Tuft, "Scattering of light from a rotating ground glass∗", J. Opt. Soc. Am. **61**, 1301–1306 (1971).

[72]E. Jakeman, "The effect of wavefront curvature on the coherence properties of laser light scattered by target centres in uniform motion", J. Phys. A **8**, L23 (1975).

[73]C. Henry, "Theory of the linewidth of semiconductor lasers", IEEE Journal of Quantum Electronics **18**, 259–264 (1982).

[74]T. A. Birks, I. Gris-Sánchez, S. Yerolatsitis, S. G. Leon-Saval, and R. R. Thomson, "The photonic lantern", Adv. Opt. Photon. **7**, 107–167 (2015).

[75]C. W. Gardiner and A. S. Parkins, "Driving atoms with light of arbitrary statistics", Phys. Rev. A **50**, 1792–1806 (1994).

[76]P. Kochan and H. J. Carmichael, "Photon-statistics dependence of single-atom absorption", Phys. Rev. A **50**, 1700–1709 (1994).

[77]M. K. Tey, Z. Chen, S. A. Aljunid, B. Chng, F. Huber, G. Maslennikov, and C. Kurtsiefer, "Strong interaction between light and a single trapped atom without the need for a cavity", Nature Physics **4**, 924–927 (2008).

[78]V. Leong, M. A. Seidler, M. Steiner, A. Cerè, and C. Kurtsiefer, "Time-resolved scattering of a single photon by a single atom", Nature Communications **7**, 13716 (2016).

[79]S. A. Gunin, A. Y. Dmitriev, A. V. Vasenin, K. S. Tikhonov, G. P. Fedorov, and O. V. Astafiev, "Quantum and classical field scattered on a single two-level system", Phys. Rev. A **108**, 033723 (2023).

[80]R. Benzi, A. Sutera, and A. Vulpiani, "The mechanism of stochastic resonance", Journal of Physics A: Mathematical and General **14**, L453 (1981).

[81]R. Bartussek, P. Hänggi, and P. Jung, "Stochastic resonance in optical bistable systems", Phys. Rev. E **49**, 3930–3939 (1994).

[82]M. Grifoni and P. Hänggi, "Coherent and incoherent quantum stochastic resonance", Phys. Rev. Lett. **76**, 1611–1614 (1996).

[83]D. Gottesman, T. Jennewein, and S. Croke, "Longer-baseline telescopes using quantum repeaters", Phys. Rev. Lett. **109**, 070503 (2012).

[84]E. T. Khabiboulline, J. Borregaard, K. De Greve, and M. D. Lukin, "Quantum-assisted telescope arrays", Phys. Rev. A **100**, 022316 (2019).

[85]E. T. Khabiboulline, J. Borregaard, K. De Greve, and M. D. Lukin, "Optical interferometry with quantum networks", Phys. Rev. Lett. **123**, 070504 (2019).

[86]D. Diaz, Y. Zhang, V. O. Lorenz, and P. G. Kwiat, "Emulating quantum-enhanced long-baseline interferometric telescopy", in Frontiers in optics + laser science 2021 (2021), FTh6D.7.

[87]M. R. Brown, M. Allgaier, V. Thiel, J. D. Monnier, M. G. Raymer, and B. J. Smith, "Interferometric imaging using shared quantum entanglement", Phys. Rev. Lett. **131**, 210801 (2023).

[88]Y. Suematsu, S. Akiba, and T. Hong, "Measurement of spontaneous-emission factor of algaas double-heterostructure semiconductor lasers", IEEE Journal of Quantum Electronics **13**, 596–600 (1977).

[89]J. Goodwin and B. Garside, "Measurement of spontaneous emission factor for injection lasers", IEEE Journal of Quantum Electronics **18**, 1264–1271 (1982).

[90]F. Grosshans and P. Grangier, "Continuous variable quantum cryptography using coherent states", Phys. Rev. Lett. **88**, 057902 (2002).

[91]D. H. Menzel, "Laser action in non-lte atmospheres", International Astronomical Union Colloquium **2**, 134–137 (1970).

[92]N. N. Lavrinovich and L. V. S., "The possibility of the laser effect in stellar atmosphere", Sov. Phys.-JETP **40**, 800–805 (1975).

[93]Y. P. Varshni and R. M. Nasser, "Laser action in stellar envelopes", Astrophysics and Space Science **125**, 341–360 (1986).

[94]V. S. Letokhov, "Astrophysical lasers", Quantum Electronics **32**, 1065 (2002).

[95]A. W. Howard, P. Horowitz, D. T. Wilkinson, C. M. Coldwell, E. J. Groth, N. Jarosik, D. W. Latham, R. P. Stefanik, J. Alexander J. Willman, J. Wolff, and J. M. Zajac, "Search for nanosecond optical pulses from nearby solar-type stars", The Astrophysical Journal **613**, 1270 (2004).

[96]I. Almár, "Seti and astrobiology: the rio scale and the london scale", Acta Astronautica **69**, 899–904 (2011).

[97]P. Morrison, J. Billingham, and J. Wolfe, "The search for extraterrestrial intelligence—seti", Acta Astronautica **6**, 11–31 (1979).

[98]D. S. Wiersma, "The physics and applications of random lasers", Nature Physics **4**, 359–367 (2008).

[99]W. Guerin, N. Mercadier, F. Michaud, D. Brivio, L. S. Froufe-Pérez, R. Carminati, V. Eremeev, A. Goetschy, S. E. Skipetrov, and R. Kaiser, "Towards a random laser with cold atoms", Journal of Optics **12**, 024002 (2010).

[100]H. K. Liang, B. Meng, G. Liang, J. Tao, Y. Chong, Q. J. Wang, and Y. Zhang, "Electrically pumped mid-infrared random lasers", Advanced Materials **25**, 6859–6863 (2013).